Acta Astronautica 234 (2025) 601–618

Contents lists available at ScienceDirect

Acta Astronautica

journal homepage: www.elsevier.com/locate/actaastro

Research paper

Analysis of the unsteady shock wave motion in inlet unstart processes

Carlos Carbajosa *, Ángel Sanz-Andrés, Alejandro Martínez-Cava, Mikel Ogueta-Gutiérrez

Instituto Universitario "Ignacio Da Riva" (IDR/UPM), Universidad Politécnica de Madrid, Plaza Cardenal Cisneros, E-28040 Madrid, Spain

ARTICLE INFO

Keywords:
Unstart
Motion speed
Shock-wave
Ramjet/scramjet
Shock-train
Pseudo-shock

ABSTRACT

This paper is focused on the shock wave motion during inlet starting and unstarting phenomena (swallowing and expelling of shock waves) on supersonic and hypersonic diffusers, which are critical for the efficient operation of both ramjets and scramjets. The motion speed of a normal shock wave along the inlet duct during these processes is analyzed to better understand the influence of design parameters, such as the Mach number (M_∞) and contraction ratio (CR), on the speed and stability behavior of the shock wave position.

A one-dimensional (1D) quasi-steady mathematical model is presented here, labeled DS^2M (*Duct Shock Speed Model*), which allows for fast approximate calculations. This simple approach is useful for analyzing how the shock wave motion speed changes along the duct as a function of the duct geometry and operating parameters. It also allows for shock wave position stability assessment around equilibrium positions. This model is also suitable for hypersonic configurations, where the set of shock waves that appears, so-called pseudo-shock, could be appropriately replaced by an equivalent normal shock, subjected to a corrected Mach number, lower than that of the original system.

In the presentation of results, both stable and unstable cases are discussed, showing how the shock wave can be swallowed or expelled depending on the evolution of the flow and duct geometry. Finally, the results obtained from the DS^2M model developed here are compared with relevant published experimental data (including shock unstart experiments on two-dimensional and three-dimensional inlets with and without combustion, as well as buzz analysis in a scramjet), showing a good agreement. Difficulties concerning the comparison exercises are outlined.

1. Introduction

The swallowing and expelling process of the shock wave system in supersonic or hypersonic inlets is a subject of great interest, as it is fundamental to the proper operation of ramjet or scramjet engines [1]. For instance, in scramjets, if the heat generated by the combustion process exceeds a critical value, the Mach number in the engine drops to unity and the flow becomes thermally choked, leading to unstart [1,2]. This swallowing and expelling process has also attracted attention in other applications, such as the unstarting phenomenon in supersonic inlet cascades [3].

Whereas in the started mode some of the shock waves are placed inside the duct, typically in the divergent region, the phenomenon of unstart occurs as a result of the expelling of some of these shock waves, and the supersonic flow inside the inlet duct is not achieved, as a consequence of the subsonic flow generated by a detached shock wave placed upstream of the inlet entrance. In ramjets and scramjets, the mass flow rate and compression ratio are entirely supplied by the inlet across a wide range of flight and operating conditions [4], requiring the best performance with minimum weight. To achieve this, the engine must operate in the started mode and avoid entering the unstarted mode [5,6].

The unstart phenomenon has been extensively studied [5,7,8] and has been found to depend on parameters such as the flight Mach number (M_∞), the contraction ratio ($CR = A_t/A_1$: throat area, A_t; inlet area, A_1), the acceleration process, and geometry changes. It also depends on the inlet angle of attack, fuel addition, overheating, and back-pressure [5,9–11].

In addition to the two operational modes previously introduced, the stability of shock wave position should be considered. This issue arises because, for a given equilibrium position (where the shock wave motion velocity is zero), the equilibrium may be either stable or unstable. This stability depends on whether small positional perturbations preserve the shock wave's position or displace it from this equilibrium. The

* Corresponding author.
E-mail addresses: c.carbajosa@upm.es (C. Carbajosa), angel.sanz.andres@upm.es (Á. Sanz-Andrés), alejandro.martinezcava@upm.es (A. Martínez-Cava), mikel.ogueta@upm.es (M. Ogueta-Gutiérrez).

https://doi.org/10.1016/j.actaastro.2025.05.006
Received 10 December 2024; Received in revised form 10 April 2025; Accepted 4 May 2025
Available online 20 May 2025

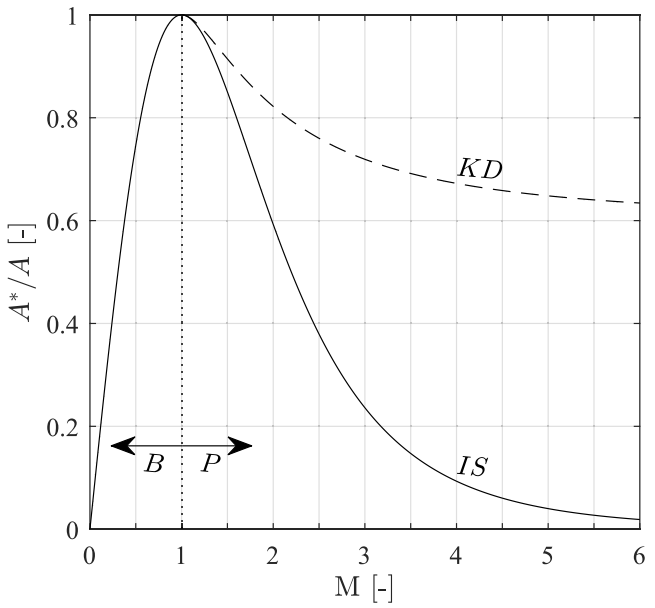

Fig. 1. Variation of the contraction ratio, $CR = A^*/A$, as a function of the Mach number in the section, M. Isentropic limit (continuous line, IS) and the Kantrowitz–Donaldson limit (dashed line, KD). Vertical dashed line at M = 1: boundary between the solution for the subsonic branch (left, B) and the supersonic branch (right, P) [8].

stability of the normal shock wave position depends on whether it is placed within a converging or diverging section of the duct. In stable cases, the flow topology (shock wave swallowed or expelled) depends on the region of the parameter space (see Figure 1, [8]) defined by CR and M_∞ where the configuration is located [4,12], however, it is affected by a hysteretic effect.

In the case of an inlet with a single throat, two limit conditions appear that mark the transition to either the started or unstarted flows. One is the Kantrowitz–Donaldson limit (KD), which occurs when the throat is choked (*i.e.*, in critical conditions) for the subsonic flow generated by the normal shock wave which is positioned precisely at the inlet entrance. Beyond this limit condition, as a consequence of a slight increase in throat area or Mach number, the autonomous swallowing of the normal shock wave is produced, eventually positioning it at one section of the divergent part of the duct. The other one is the isentropic limit (IS), where the flow is decelerated from the supersonic incoming flow at the entrance till reaching critical conditions at the throat. It arises when, with the normal shock wave already positioned inside the inlet, the throat is gradually narrowed, or the Mach number of the incoming flow is progressively reduced while controlling the pressure at the exit, so that the shock wave is maintained at the throat. This can be continued until reaching a condition without a normal shock wave, with the throat operating at sonic conditions. If the throat area, or the Mach number is further reduced, the configuration can no longer be maintained.

As summarized in Fig. 1, the normal shock wave can be either expelled (below the IS limit) or swallowed (above the KD limit), and an intermediate region appears (in the space between the KD and IS limits) where the configuration depends on the previous flow evolution. If there is more than one throat (for example, if a flow control valve is added at the rear), three flow patterns emerge, and the stability configuration diagram becomes significantly more complex [13]. In unstable cases, which appear when the boundaries of the hysteresis region are reached from stable configurations, leading to the swallowing or expelling of the normal shock, the shock wave will propagate across the duct, either upstream or downstream, depending on the previous flow topology.

Throat choking, which occurs when sonic conditions are attained at the throat, leads to unstart. The presence of a heat addition process in the combustion chamber can raise the rear pressure (back-pressure), which can be associated with a reduction in the equivalent critical throat area. Notably, depending on parameters such as the Mach number, equivalence ratio, and expansion ratio, a scramjet combustor (and consequently the entire propulsion system) can operate within one of three distinct regimes: a high-performance stable regime, a low-performance stable regime, or an unstable regime [14].

As the problem considered involves several aspects, they are addressed in the remainder of this introduction, organized as follows:

1. Summary of existing theoretical shock wave motion models, with the aim of giving a review of the most relevant previous work regarding theoretical models.
2. The unstart phenomenon, which is the main application field and source of experiments for validation of the model developed.
3. Experimental results on shock wave motion during inlet unstart, which allows the validation of the developed model and also include the need for modelization of the experiments.
4. Application of the DS^2M model to high supersonic and hypersonic inlets (based on the concept of pseudo-shock).

1.1. Summary of existing theoretical shock wave motion models

To determine the complexity level required for this study, the existing models of shock wave motion should be considered. In fact, research on the motion of finite and shock waves in open flows or ducts, where the medium is either stationary or in motion, through analytical models in 1D, 2D, or 3D configurations, has captured the attention of many researchers.

The abovementioned IS and KD limits for establishing supersonic flow within a convergent–divergent nozzle were studied by Kantrowitz and Donaldson [12]. Additionally, the stability of a shock wave positioned near the throat in response to downstream-generated disturbances was analyzed by Kantrowitz [15], yielding results pertinent to the current problem. When the shock wave is ingested by the inlet, steady-state solutions both upstream and downstream of the shock wave can be employed. The downstream region comprises subsonic flow up to the inlet throat, which operates at critical conditions, while the upstream region allows for a supersonic solution along the inlet duct that feeds the normal shock wave. Furthermore, various conditions were examined to assess the influence of acoustic waves generated by the motion of the normal shock wave propagating along the subsonic portion of the flow [12,15], particularly as they are reflected at the critical throat. It was concluded that their influence is not highly significant.

In addition, the motion of shock waves within a medium at rest with respect to the duct was examined by Whitham [16] following Chester [17]. This approach, known as the CCW method, builds on the work of Chester [17], Chisnell [18], and Whitham [19]. However, a different case arises when the shock wave moves through a duct already containing fluid flow, particularly when area variations are present, as in an air inlet. This initial fluid motion has its own characteristics (shock wave position, critical throats, etc.).

The problem of one-dimensional shock wave motion within a moving fluid in a duct was analyzed by Han and Yin [20], using generalized CCW methods that extend Chester's framework [17]. Chester's extension of Whitham's original method, initially applied to uniform width channels in a quiescent gas ahead of a shock, was adapted to cases involving gases moving in non-uniform width channels [21].

In his doctoral thesis, Rabi Tahir [22] proposed adjustments to the KD limit for cases involving an oblique shock within a diffuser (allowing for self-starting at off-design conditions), providing a comprehensive overview of shock wave motion under various conditions.

The mentioned theoretical models, which include the generation and motion of finite or acoustic waves, provide a detailed study of the problem but are excessively complex for our purpose. Additionally, since we only consider those cases where the motion speed of moving shock waves is small (approximately 0.1 M_∞), it is possible to disregard the potential effects of finite or acoustic waves generated by changes in shock wave intensity caused by area changes due to the displacement of the normal shock wave.

1.2. The unstart phenomenon

When the shock wave is expelled from the inlet, subcritical operation arises, with the risk of buzz, a phenomenon characterized by the rapid motion of shock waves [5], as well as interaction with viscous phenomena such as boundary layer separation.

The operational challenges associated with supersonic diffusers have been extensively analyzed in studies by JHU-APL [23], Seddon and Goldsmith [24], and Van Wie [4] among others. To address the requirement for a larger effective flow area during startup, as constrained by the KD limit, several strategies have been proposed. These include the implementation of perforated inlets [25–27] and the application of air injection or energy deposition techniques to mitigate separation bubbles at the cowl, thereby increasing the critical back-pressure and delaying flow unstart [28–30]. Additionally, the use of advanced control algorithms to manage the inlet angle of attack and its rate of change during flight has been shown to effectively prevent the onset of unstart phenomena [31].

The distinction between soft unstarts (resulting from detached flow) and hard unstarts (caused by throat blockage) was established by Van Wie, Kwok, and Walsh [32], who also provided an empirical limit for the maximum allowable contraction for Mach numbers ranging from 2.5 to 10. It was demonstrated that the KD limit effectively predicts hard unstarts.

The unstart process was also experimentally analyzed by Wagner et al. [33,34], who identified several oscillatory regimes that follow unstart and provided data on shock motion speed.

Rabi Tahir [22] proposed several models for shock wave motion, including a model for "impulsive flow starting", alongside a comprehensive review.

A formulation based on catastrophe theory, which allows studying inlets with several throats, was developed by Tao et al. [35], which will be used in Section 4.2. Throckmorton and Schetz [36] employed experimental and numerical methods to analyze a startup system for a two-dimensional scramjet inlet with a variable contraction ratio, utilizing a dynamic gate, in order to facilitate start. An empirical equation for autonomous startup, valid for Mach numbers between 1.65 and 4.68, was derived by Sun and Zhang [37]. Cui, Lv, and Yu [13] introduced a new perspective by incorporating system dynamics to investigate mechanisms of stability change in the unstart phenomenon.

A review of different types and causes of unstart initiation, including its detection and control, can be found in Chang et al. [5], who analyzed various hysteresis processes. The complete inlet-combustor system was analyzed by Zvegintsev [6] as part of an extensive review complementary to [5].

An alternative to the KD limit was proposed by Xie et al. [38], who considered viscous effects. While viscosity influences the resulting curves, the general trends remain consistent. It was noted that although viscosity is significant in detailed design and operational phases, it can be neglected during preliminary design, justifying the use of a non-viscous model like the one presented here.

Finally, Jin et al. [39] conducted a numerical study on the flow response hysteresis problem in a two-dimensional mixed-compression supersonic inlet. Their findings revealed that two throats (one aerodynamic and one geometric) emerge, leading to a complex hysteresis behavior. The implications of the presence of two throats can be analyzed using the results of Tao et al. [35] (see Section 4.2).

Table 1
Summary of the key parameters from the experimental studies available in the literature used to validate the DS^2M model.

Configuration	M_∞	Shock motion speed [m/s]	Reference
2D single-throat	4.9	19–37	Wagner *et al.* [33,34]
2D double-throat	4.0	55–70	Rodi *et al.* [41]
3D single-throat	5.3	27	Wieting *et al.* [40]
Scramjet with combustion	5.5	75–150	O'Byrne *et al.* [2]
Scramjet with buzz	4.9	80–130	Tan *et al.* [42,43]

1.3. Experimental results on shock wave motion during inlet unstart

Amongst the comprehensive literature on experimental studies (see reviews [5,7,8]), concerning experimental data on shock speeds during inlet start or unstart, only a few references have been acknowledged [2, 33,34,40–43]. In most of these cases, speed is derived from the time delay between signals recorded by contiguous pressure probes. These references are highlighted here, and are further analyzed in Section 4 (see Table 1).

Upstream shock motion speed data at various locations within an inlet during unstart were reported by Wagner et al. [33,34]. By employing Schlieren visualization, these authors analyzed and compared pressure distribution data with shock positions, identifying regions of subsonic and supersonic flow. The experimental results obtained were successfully replicated numerically by Lee and Kang [44].

A ramjet/scramjet with an adjustable-angle lip was studied by Rodi, Emami, and Trexler [41], where the back-pressure effect from combustion was simulated by using a valve to close the duct, observing its effect on the onset of unstart.

The transients during scramjet unstart were investigated by Wieting [40] by blocking the duct exit with a pin to determine the mechanical loads on the structure. The geometric configuration, being three-dimensional and complex, was found to complicate the establishment of an equivalent one-dimensional model.

Shock wave motion speeds for various fuel–air equivalence ratios were determined by O'Byrne et al. [2], who noted that "heat release may act as a physical flow restriction, in the same way a blockage in the duct might cause the supersonic flow to become mechanically choked. This assumption had been considered in earlier studies on thermal choking in scramjet combustors [41]". While some interesting conclusions were drawn, these experimental results cannot be directly applied here, as the relationship between the critical equivalent area generated by combustion and the fuel–air ratio was not established by these authors.

The oscillatory instability known as buzz was analyzed by Tan et al. [42,43], who provided the fundamental oscillation frequencies for different contraction ratios. This data can be used to determine the mean shock motion speed through a simplified approach (see Section 4).

1.4. Application of the DS^2M model to high supersonic and hypersonic inlets

The question is if it is possible to generalize the results presented in this paper to hypersonic inlets, considering that in such large diffusers, a normal shock does not form, but rather a set of shock waves known as a pseudo-shock [45]. The model developed here is based on the presence of a single, mobile normal shock wave, which is typical for flow in ducts at moderate Mach numbers. However, for larger Mach numbers, such as those encountered in hypersonic diffusers, a system of shock waves may form in the rear of the diffuser. This system, known as a shock train, is followed by a subsonic deceleration, collectively referred to as a pseudo-shock, challenging the modelization as a single equivalent shock wave.

A hypersonic diffuser is characterized by the presence of an isolator, introduced to stabilize the flow in such engines [1,8]. This isolator is

a constant-section duct, several times the diameter in length, located between the inlet and the combustor (see Figure 27 of [45]). In dual-mode ramjet/scramjet operation, the geometry of the diffuser duct remains fixed, with two fuel injectors [45], one placed before (for scramjet operation), and the other one after (for ramjet operation) the isolator. As abovementioned, in a long duct (*e.g.*, the isolator or the rear diffuser), instead of a single normal shock wave, a shock train or pseudo-shock may appear. The shock wave configuration depends on the incoming Mach number (see Figure 8 of Tamaki et al. [46], Figure 25 of Matsuo et al. [45], and Figure 1 of Sajben et al. [47]) and the back-pressure ratio (Figures 13 and 14 of Soltani et al. [48]). The complexity of the interaction between shock waves and boundary layers in various configurations has been described by Huang et al. [8], considering both the front part of the inlet (generated by compression ramps, known as background waves) and the interaction with the rear shock train, as well as the oscillations generated by their interaction with the boundary layer.

To compare the effect of the pseudo-shock wave system with a single equivalent normal shock, the pressure jump was considered for both cases (see Figures 6 and 9 of Tamaki et al. [46], and Figures 4, 6, and 9 of Matsuo et al. [45]), as a function of the Mach number. The comparison can be considered satisfactory if, instead of using the entry Mach number, a corrected, lower Mach number is taken into account. Such a generalized normal shock wave model is used for analyzing the effect of a pseudo-shock (see Section 5.1 of Tamaki et al. [46]), which includes the friction effect in the duct area where the pseudo-shock is placed.

The above discussion refers to a steady process. However, the unstart process can be considered steady in the supersonic part of the flow, and unsteady in the subsonic section of the flow (between the end of the supersonic portion of the pseudo-shock and the inlet exit). Indeed, a steep static pressure gradient develops in the subsonic section to slow the fluid, helping to reduce the flow passing through the blocked throat (see Figures 9 and 11 of Wagner et al. [34]). This gradient could be associated with the gradual pressure increase along the pseudo-shock, which disappears when the shock wave is expelled, causing a sudden spillage and reducing the mass flow through the inlet.

1.5. Contributions and structure of the paper

This paper is focused on studying the motion speed of the normal shock wave relative to the inlet during the swallowing and expelling processes, in order to analyze the influence of the configuration parameters on the stability or instability of the shock wave position. To this end, a basic description is employed, and a simple one-dimensional (1D) quasi-steady model (an approach frequently used [49]), herein called DS^2M model (which stands for *Duct Shock Speed Model*), is developed considering a normal shock wave, which allows us to simplify the formulation, based on quick approximate calculations. To perform the analysis, the dependence of the shock speed on the throat area is considered, as well as a specific duct geometry, to determine the shock motion speed along the entire duct, for different points on the $CR-\mathrm{M}_\infty$ diagram, in order to explain the various types of flow evolution (see Section 2). In Section 3, the DS^2M model results and discussion are outlined.

In addition, unstarts induced by back-pressure increase or heat release can also be analyzed using the DS^2M model, as they are equivalent to reducing the effective critical area of the final throat. Thus, the results of this study could also be applied to explain unstart caused by intense combustion [2]. Besides, it would be interesting to analyze the conditions under which the DS^2M model developed here could be applied to the cases of high supersonic and hypersonic diffusers, if only qualitatively, by substituting the pseudo-shock with an equivalent normal shock wave, as long as there is a slow enough throat closure. This assumption is valid if $t_c \ll t_r$, being t_c the characteristic closure time, and $t_r \sim L_{char}/a_\infty$ the residence time for a fluid particle

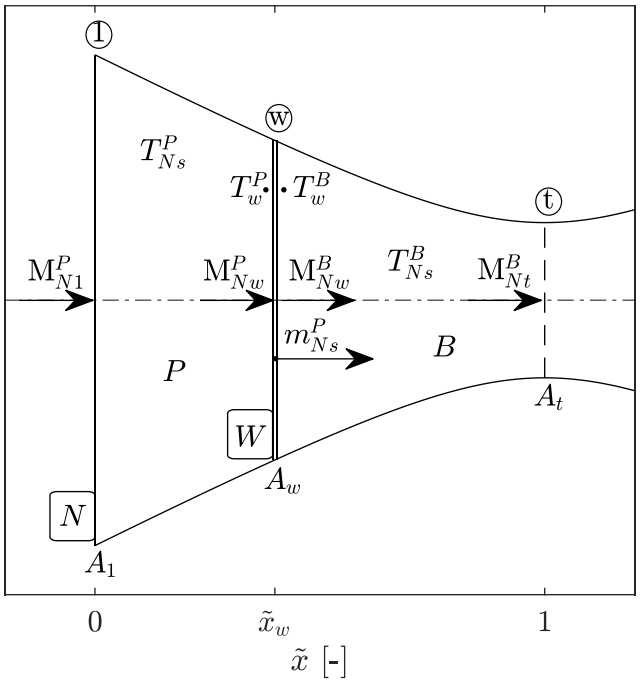

Fig. 2. Sketch of the inlet considered. The throat, A_t, is assumed to be at critical conditions. Nomenclature: see Appendix A. *P* and *B*: supersonic and subsonic branches, respectively.

(where L_{char} is the characteristic inlet length, and a_∞ is the reference sound speed). In Section 4, the previous assumptions are evaluated and the DS^2M model is validated by using the results obtained in the experimental tests mentioned in Section 1.3. Finally, in Section 5, conclusions are drawn.

2. Mathematical formulation

2.1. General problem statement

The aim of this work is to analyze the transient motion of a shock wave within an air inlet duct (see Fig. 2), specifically, considering the shock wave motion speed as a function of its position. To this end, the DS^2M analytical model is presented in this section.

To address the problem, the Mach number and total temperature at the inlet entrance, M^P_{N1} and T^P_{Ns} respectively, are considered known, as well as the area distribution of the inlet, $A(x)$, as a function of the longitudinal distance from the entrance, x. The area distribution can be expressed in dimensionless form as:

$$\eta(\tilde{x}) = A(\tilde{x})/A_1 \leq 1, \quad \text{with} \quad \tilde{x} = x/L, \tag{1}$$

where A_1 represents the entrance area, $\tilde{x} = x/L$ is the dimensionless longitudinal position, and L is the longitudinal distance between the entrance and the throat. The dimensionless areas of the sections at the throat and the shock wave position are:

$$\eta_t = A_t/A_1 \quad \text{and} \quad \eta_w = A_w/A_1, \tag{2}$$

respectively. Accordingly, the dimensionless results will depend on (see Fig. 2): the Mach number at the entrance, M^P_{N1}; the position of the shock wave, $\tilde{x}_w$; and the dimensionless geometry of the inlet, $\eta(\tilde{x})$. However, the latter two dependencies can be replaced by dependencies on η_w and η_t. When providing dimensional results, the dependencies will generally include: the total temperature at the entrance in the reference frame fixed to the inlet, T^P_{Ns}; the longitudinal distance between the entrance and the throat, L; and the inlet area at the entrance section, A_1. These dependencies are generally omitted throughout the text to simplify the notation.

2.2. Nomenclature

Nomenclature is summarized in Appendix A. The quantities considered will generally be evaluated at three positions: the entrance ($_1$), the throat ($_t$), and the position of the shock wave ($_w$). Additionally, the quantities may refer to either the supersonic branch (^{P}) or the subsonic branch (^{B}), or be defined in a reference frame attached to the inlet ($_N$) or to the shock wave ($_W$). Some quantities may be total or stagnation quantities ($_s$), which are dependent on the reference frame in which they are expressed. For quantities which are independent of the reference frame, like static temperature, no subscript is used. The configuration considered and the nomenclature employed are shown in Fig. 2.

2.3. Assumptions

According to the references included in the introduction (see Section 1), the following assumptions are considered:

- *Planar and infinitesimal shock wave*: The shock wave is assumed to be planar and infinitesimally thin, neglecting the modeling of its internal structure.
- *One-dimensional motion*: The fluid flow is assumed to depend only on the longitudinal coordinate x, disregarding any two- or three-dimensional effects.
- *Quasi-steady fluid motion*: Since the shock wave motion speed is small compared to the speed of sound, the flow is assumed to adapt almost instantaneously to the shock position inside the inlet, such that the steady flow conditions at both sides of the shock are met. The supersonic flow upstream of the shock remains steady as it is undisturbed, while the subsonic flow downstream the shock is considered quasi-steady (small shock speed and acceleration).
- *Absence of acoustic waves*: The shock wave speed is assumed to be much lower than the speed of sound, allowing for neglecting the effect of acoustic waves (in the subsonic region between the shock and the throat) caused by the shock motion.
- *Isentropic flow*: External heat input is neglected throughout the entire fluid field, and irreversibilities are assumed only at the shock wave itself.
- *Isenthalpic flow in the shock-fixed reference frame, W*: It is assumed that, in addition to the absence of external heat input, no work is done on the fluid in the shock-fixed frame, thus preserving total enthalpy. Thus, the total temperature remains constant upstream and downstream the shock in this frame, W. However, this cannot be assumed in the frame fixed to the inlet, N, where total temperatures jump across the shock, *i.e.*, $T^P_{Ns} \neq T^B_{Ns}$ (see Appendix B).

2.4. Equations and solution of the problem: shock motion speed

With the proposed assumptions, the equations required to solve the problem are formulated as follows. For the flow upstream and downstream of the shock wave, considering a steady, one-dimensional isentropic flow in a duct, the function relating the area at each section, A, to the Mach number at the section, M, is given by [4]:

$$\frac{A(\mathrm{M})}{A^*} = \frac{1}{\mathrm{M}}\left[\frac{2}{\gamma+1}\left(1+\frac{\gamma-1}{2}\mathrm{M}^2\right)\right]^{\frac{\gamma+1}{2(\gamma-1)}}, \tag{3}$$

where A^* is the critical area, and γ is the air specific heat ratio. The above expression has two branches, depending on whether the Mach number is subsonic ($\mathrm{M} \leq 1$) or supersonic ($\mathrm{M} \geq 1$), the critical area being different upstream and downstream of the shock. Indeed, upstream of the shock (supersonic flow), is $A^* \equiv A^{P*} = A^*_1$, while downstream of the shock (subsonic), it is $A^* \equiv A^{B*} = A_t$. The isentropic evolution given by Eq. (3) for $\mathrm{M} > 1$ is shown in Fig. 1 (curve IS).

Concerning the motion of the shock in the duct, the conditions at both sides upstream and downstream the shock must satisfy the Prandtl's relationship between the Mach number of the flow incident on the shock, M_i, and the Mach number of the flow exiting the shock, M_d, in coordinates attached to the shock wave itself, W:

$$\mathrm{M}_d(\mathrm{M}_i) = \sqrt{\frac{1+\frac{\gamma-1}{2}\mathrm{M}_i^2}{\gamma\mathrm{M}_i^2-\frac{\gamma-1}{2}}}, \quad \text{with } \mathrm{M}_i \geq 1. \tag{4}$$

From Eqs. (3) and (4), and using the corresponding isentropic flow relations, the problem of determining the shock speed can be solved. Let us consider first the flow in the supersonic region P. To do so, the critical area A^*_1 corresponding to the supersonic flow is obtained using Eq. (3) (isentropic supersonic flow up to the shock wave):

$$\frac{A_1}{A^*_1} = \frac{1}{\mathrm{M}^P_{N1}}\left[\frac{2}{\gamma+1}\left(1+\frac{\gamma-1}{2}\left(\mathrm{M}^P_{N1}\right)^2\right)\right]^{\frac{\gamma+1}{2(\gamma-1)}}. \tag{5}$$

If it is assumed that, at a given instant, the shock is placed within the inlet at a distance $\tilde{x}_w$ from the entrance, the supersonic Mach number at the position of the shock in reference frame N, M^P_{Nw} $\left[=\mathrm{M}^P_{Nw}(\eta_w;\mathrm{M}^P_{N1}) \geq 1\right]$, can be obtained as a function of the section area at the shock position, $\eta_w = \eta(\tilde{x}_w)$, and the entry Mach number, M^P_{N1}, from the implicit equation:

$$\frac{A(\mathrm{M}^P_{Nw})}{A^*} = \frac{A_1}{A^*_1}\eta_w. \tag{6}$$

For the subsonic flow just downstream the shock, assuming that the throat is always in critical conditions, $A_t = A^{B*}$, the subsonic Mach number in coordinates fixed to the inlet, $\mathrm{M}^B_{Nw} = \mathrm{M}^B_{Nw}(\eta_w;\eta_t) \leq 1$, can be obtained by solving the implicit Eq. (3) using A/A^* given by:

$$\frac{A(\mathrm{M}^B_{Nw})}{A^*} = \frac{\eta_w}{\eta_t}. \tag{7}$$

The stagnation temperature in reference frame N is conserved from the entry to the upstream side of the shock, so the ratio between the stagnation temperature ahead of the shock, T^P_{Ns}, and the static temperature just at the shock, T^P_w, is given by:

$$\frac{T^P_{Ns}}{T^P_w} = 1+\frac{\gamma-1}{2}\left(\mathrm{M}^P_{Nw}\right)^2, \tag{8}$$

where the Mach number at that position, M^P_{Nw}, is obtained from Eq. (6) as a function of $\eta_w = \eta(\tilde{x}_w)$ and M^P_{N1}.

Besides, the fluid speed in reference frame N, V_N, can be related to its speed in reference frame W, V_W, simply by accounting for the shock motion speed, $\dot{x}_w$, taking it as positive when the shock moves from the entrance towards the throat, as:

$$\begin{aligned} V^P_W &= V^P_N - \dot{x}_w, \quad \text{and} \\ V^B_W &= V^B_N - \dot{x}_w, \end{aligned} \tag{9}$$

for the supersonic and subsonic flows, respectively.

Eq. (9) can be made dimensionless by using the speed of sound just upstream, $\sqrt{\gamma R_g T^P_w}$, and downstream the shock, $\sqrt{\gamma R_g T^B_w}$, respectively, where R_g is the specific gas constant for air. Additionally, it should be noted that the static temperature at both sides of the shock depends only on the shock position and the branch (supersonic or subsonic) considered, regardless of the reference frame used. Thus, considering the shock motion speed, a Mach number associated with the shock motion in N reference frame referred to the stagnation sound speed of the supersonic region P can be introduced:

$$m^P_{Ns} = \frac{\dot{x}_w}{\sqrt{\gamma R_g T^P_{Ns}}}. \tag{10}$$

Now, Eq. (9) takes the form:

$$\mathrm{M}^P_{Ww} = \mathrm{M}^P_{Nw} - \sqrt{\frac{T^P_{Ns}}{T^P_w}}m^P_{Ns}, \quad \text{and} \tag{11}$$

$$\mathrm{M}^{B}_{Ww} = \mathrm{M}^{B}_{Nw} - \sqrt{r_{Ts}}\sqrt{\frac{T_{Ws}}{T^{B}_{w}}}m^{P}_{Ns}, \tag{12}$$

respectively, where the stagnation temperature ratio is defined as:

$$r_{Ts} \equiv \frac{T^{P}_{Ns}}{T_{Ws}}. \tag{13}$$

Note that, at this point, the value of the ratio r_{Ts}, as well as the ratio T_{Ws}/T^{B}_{w}, is unknown. The conservation of stagnation temperature in reference frame W allows us to write:

$$\frac{T_{Ws}}{T^{P}_{w}} = 1 + \frac{\gamma-1}{2}\left(\mathrm{M}^{P}_{Ww}\right)^2 = 1 + \frac{\gamma-1}{2}\left(\mathrm{M}^{P}_{Nw} - \sqrt{\frac{T^{P}_{Ns}}{T^{P}_{w}}}m^{P}_{Ns}\right)^2, \tag{14}$$

where M^{P}_{Ww} is given by Eq. (11). By dividing Eq. (8) by Eq. (14), we obtain:

$$r_{Ts} \equiv \frac{T^{P}_{Ns}}{T_{Ws}} = \frac{1 + \frac{\gamma-1}{2}\left(\mathrm{M}^{P}_{Nw}\right)^2}{1 + \frac{\gamma-1}{2}\left(\mathrm{M}^{P}_{Nw} - \sqrt{\frac{T^{P}_{Ns}}{T^{P}_{w}}}m^{P}_{Ns}\right)^2}. \tag{15}$$

It can be verified that, if the shock speed is zero, then the stagnation temperature ratio becomes $r_{Ts} \equiv T^{P}_{Ns}/T_{Ws} = 1$, as expected. To determine the ratio between the stagnation temperature in the shock wave frame, T_{Ws}, and the static temperature just downstream of the shock wave, T^{B}_{w}, the conservation of stagnation temperature in the shock wave frame, W, can be rewritten as:

$$\frac{T_{Ws}}{T^{B}_{w}} = 1 + \frac{\gamma-1}{2}\left(\mathrm{M}^{B}_{Nw} - \sqrt{r_{Ts}}\sqrt{\frac{T_{Ws}}{T^{B}_{w}}}m^{P}_{Ns}\right)^2, \tag{16}$$

which is solved to find T_{Ws}/T^{B}_{w} in the form:

$$\sqrt{\frac{T_{Ws}}{T^{B}_{w}}} = \frac{(\gamma-1)\sqrt{r_{Ts}}m^{P}_{Ns}}{2\left(1 - \frac{\gamma-1}{2}r_{Ts}m^{P}_{Ns}\right)} \times \left(-1 \pm \sqrt{1 + 4\frac{\left(1 - \frac{\gamma-1}{2}r_{Ts}m^{P}_{Ns}\right)\left(1 + \frac{\gamma-1}{2}\left[\mathrm{M}^{B}_{Nw}\right]^2\right)}{\left((\gamma-1)\sqrt{r_{Ts}}m^{P}_{Ns}\right)^2}}\right), \tag{17}$$

where the positive branch, +, is selected to ensure that $\sqrt{T_{Ws}/T^{B}_{w}} > 0$. Using Eqs. (15) and (16), the Mach numbers for the flow (both subsonic and supersonic) relative to the shock, M^{B}_{Ww} and M^{P}_{Ww}, can be determined by Eqs. (11) and (12), respectively, in terms of the four variables $(\eta_w, m^{P}_{Ns}; \mathrm{M}^{P}_{N1}, \eta_t)$. With these results, Prandtl's relationship given by Eq. (4) can be applied:

$$\mathrm{M}^{B}_{Ww} = \sqrt{\frac{1 + \frac{\gamma-1}{2}\left(\mathrm{M}^{P}_{Ww}\right)^2}{\gamma\left(\mathrm{M}^{P}_{Ww}\right)^2 - \frac{\gamma-1}{2}}}. \tag{18}$$

Eqs. (11), (12) and (18) form an implicit system, which can be solved to determine the dimensionless motion speed of the shock wave, m^{P}_{Ns}, in terms of the entry Mach number M^{P}_{N1} and the area ratios η_w and η_t (*i.e.*, $m^{P}_{Ns} = m^{P}_{Ns}(\eta_w; \mathrm{M}^{P}_{N1}, \eta_t)$). Besides, the dimensional motion speed of the shock can be obtained using:

$$\dot{x}_w(\eta_w; \mathrm{M}^{P}_{N1}, T^{P}_{Ns}, \eta_t) = \sqrt{\gamma R_g T^{P}_{Ns}}m^{P}_{Ns}(\eta_w; \mathrm{M}^{P}_{N1}, \eta_t). \tag{19}$$

There is a jump of the stagnation enthalpy across the shock wave in reference frame N, as is shown in Appendix B. The procedure to determine the acceleration and trajectory of the normal shock wave once its motion speed is known is described in Appendix C.

2.5. Solution method

The problem set in terms of Eqs. (11), (12) and (18) is mathematically well-posed. The solution is obtained using the numerical algorithm *fzero* available in *MATLAB*, which was selected due to the highly nonlinear nature of the equations. Due to the high nonlinearity, solving Eq. (18) along with Eqs. (11) and (12) presents certain complexities. In particular, the physically consistent solution must be chosen among all possible solutions. Details are provided in Appendix D.

3. Results and discussion

Since the motion speed of the normal shock wave depends on the dimensionless area of the section where it is located, η_w, as well as the dimensionless throat area of the duct geometry employed, η_t, and the Mach number at the inlet, M^{P}_{N1}, the main results can be summarized in just one graph as Fig. 3, where the surfaces for $\mathrm{M}^{P}_{N1} = 2.0$ and 3.0 are depicted. The grids depicted over each surface correspond to the curves $\eta_t = \text{const.}$, and $\eta_w = \text{const.}$. For a given inlet duct geometry, the dimensionless throat area η_t is fixed, so that the evolution of a shock wave follows the corresponding $\eta_t = \text{const.}$ curve. The position of the representative point η_w of the shock along the $\eta_t = \text{const.}$ curve can be obtained using first Eq. (C.4) of Appendix C to determine x_w. Then, the dimensionless area corresponding to x_w can be obtained from the inlet duct geometry definition, $\eta_w(x_w)$.

It can be observed that for sections with an area smaller than the throat, $A_w < A_t$, no solution exists. The diagonal line limits the region $A_w \geq A_t$ where solutions are possible. The region with negative motion speeds (shock being expelled) is separated from the region with positive motion speeds (shock being swallowed) by the zero-speed curve $\mathcal{Z}$, where each surface $\mathrm{M}^{P}_{N1} = \text{const.}$ intersects the plane $\dot{x}_w = 0$. A normal shock wave whose representative position is located on this curve is in unstable equilibrium if it is placed within a converging section of the duct as, if it drifts towards the throat (smaller areas), $\dot{x}_w > 0$, then it will keep on moving, and vice versa. Besides, considering the shock is located in the $\mathcal{Z}$ curve at a given η_w position, if the throat area η_t is changed, the representative point will move along the corresponding $\eta_w = \text{const.}$ curve. In this condition, if η_t is increased, then $\dot{x}_w > 0$ and, therefore, the shock will move towards the throat. If η_t is decreased, then $\dot{x}_w < 0$ and the shock will be expelled. Therefore, if a normal shock wave could be located in the converging section, it would either be swallowed or expelled, depending on whether its representative point is positioned to the left or right of the $\mathcal{Z}$ curve. This curve is the boundary between the shock wave swallowing and expelling.

Curve $\mathcal{Z}$ is limited by points IS and KD, which are the limits of unstable behavior, as defined by the IS and the KD curves in Fig. 1.

Limit IS: At the smallest A_w value, the $\mathcal{Z}$ curves intersect the diagonal (where $A_w = A_t$) as the shock wave is placed just at the throat. This solution is referred to as isentropic because, under these conditions, the Mach number incident on the shock wave at the throat is 1.0 (considering $A_t = A^{*P}$), meaning that there is no loss of entropy across the entire inlet. However, this equilibrium condition is unstable. Indeed, since the shock wave is at the throat, any perturbation will move it to a position with a larger area, associated with a negative motion speed, as shown in Fig. 3. If this motion takes place in a converging section, it would lead to unstart.

Limit KD: At the largest A_w value, the shock wave is located right at the entrance, $\eta_w = 1$. In this position, it can be observed that a small decrease in the throat area generates negative motion speeds, eventually leading to a detached shock wave placed ahead of the inlet. However, a small perturbation that moves the shock into the inlet (into a section with $\eta_w < 1$) or a slight increase in the throat area, η_t, leads to the swallowing of the shock wave thanks to the positive motion speeds. For values of $\eta_t > (\eta_t)_{KD}$, the shock wave at the inlet, $\eta_w = 1$, would have a positive speed, $\dot{x}_w > 0$, so the shock would be swallowed and settle in the divergent section of the duct, in a stable equilibrium position. For values of $\eta_t < (\eta_t)_{IS}$, the motion speed is always negative, $\dot{x}_w < 0$, so the shock waves would be expelled.

Hysteresis region: Between these two limits, the shock can either be swallowed or expelled depending on its initial condition. The shock will not be swallowed (if located at the inlet) until $\eta_t > (\eta_t)_{KD}$ and, if it is

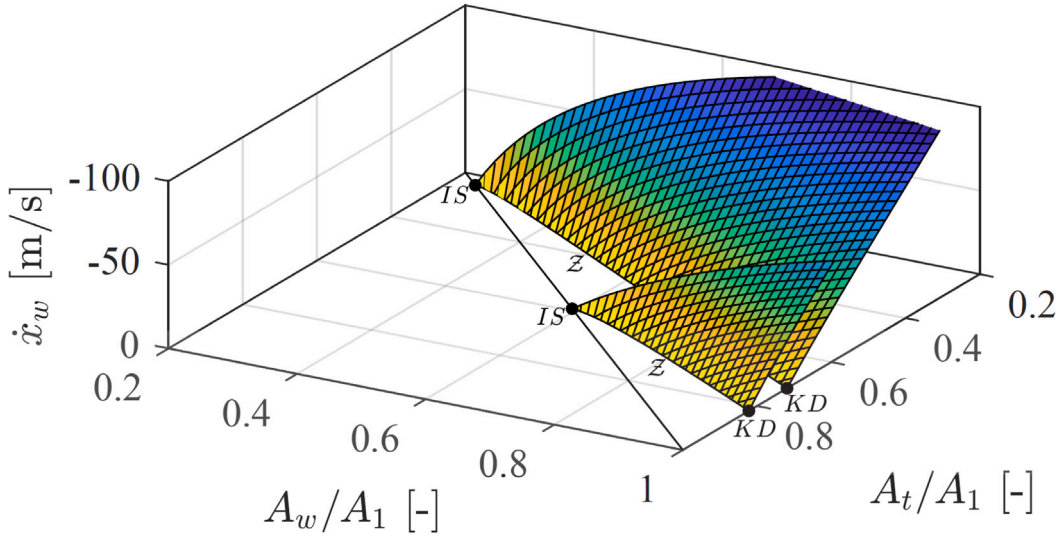

Fig. 3. Motion speed of a normal shock wave, $\dot{x}_w$, as a function of the dimensionless area of the section at the shock position, A_w/A_1, and the dimensionless throat area, A_t/A_1, for entrance Mach numbers, M^P_{N1}, of 2.0 (front) and 3.0 (rear). Stagnation temperature at the entrance $T^P_{Ns} = 290$ K. For clearness, the ingestion speeds, $\dot{x}_w > 0$, are not shown, as they lie below the $\dot{x}_w = 0$ plane. $\mathcal{Z}$: Zero-speed curves.

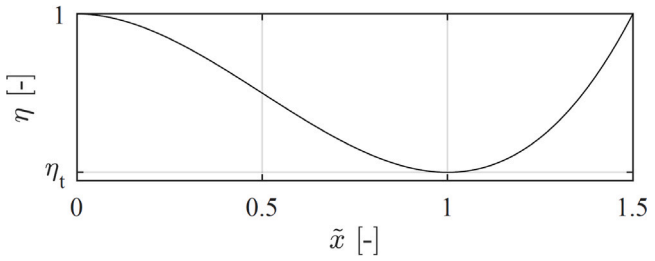

Fig. 4. Sample inlet geometry area law considered.

within the duct (in the divergent section or at the throat), it will not be expelled until $\eta_t < (\eta_t)_{IS}$. Thus, between the KD and IS limits, there is a hysteresis region.

Finally, as shown in Fig. 3, as the Mach number increases, the surfaces $M^P_{N1} = \text{const.}$ drift backwards, moving both the IS and KD limits towards smaller throat areas.

To illustrate this phenomenon, the following sample inlet geometry is proposed (see Fig. 4):

$$\eta(\tilde{x}) = A(\tilde{x})/A_1 = 1 + 6\xi\left(\frac{\tilde{x}^3}{3} - \frac{\tilde{x}^2}{2}\right), \tag{20}$$

where $\xi = 1 - \eta_t$. This law has zero derivative at both the entrance ($\tilde{x} = 0$) and the throat ($\tilde{x} = 1$).

Using this geometry, the curves representing the dimensionless motion speed of the normal shock wave are shown in Fig. 5-(a) for a fixed Mach number at the inlet and different values of the throat area. Two characteristic curves are shown: IS and KD. The curve corresponding to the IS limit shows always negative speeds (shock expelling), except when it is at the throat where the motion speed is zero (but in unstable equilibrium). For the KD limit, the motion speed is always positive (shock swallowing) except at the entrance, where the speed is zero (but in unstable equilibrium). These lines divide the space into three regions. In the region below the IS curve, where no solution exists near the throat, the shock is always expelled. In the region between both curves, there is a sign change, so spontaneous start does not occur, but if the shock is placed sufficiently inside the inlet, start will occur. Finally, in the region above the KD limit, spontaneous start (autonomous swallowing) of the shock occurs. The point $\mathcal{L}$ indicates that there is a limit where $A_w = A^{P*}$, because no solution exists for areas smaller than the critical area of the supersonic branch.

Fig. 5-(b) provides curves depicting the dimensionless motion speed of the normal shock wave, m^P_{Ns}, for a fixed throat area and different values of the Mach number at the entrance. In the specific case of Fig. 5-(b), as the motion speed is always positive, the values increase (the shock wave is swallowed faster).

Note that the dimensionless speeds m^P_{Nw} are a small fraction of the incident Mach number (for moderate values of M^P_{N1}), supporting the validity of this hypothesis.

To explore the shock behavior beyond the throat in the divergent side of the duct, the dimensionless motion speed of the shock wave is shown in Fig. 6 for configurations with A_t/A_1 at the IS limit and the KD limit for $\tilde{x}_w < 1.6$ for the sample inlet (depicted in blue in the same figure). To do this, a second throat with the same area as the first one has been assumed. The regions previously discussed in Fig. 5-(a) are shaded in red, orange, and green, corresponding to no swallowing, hysteresis, and autonomous swallowing of the shock wave, respectively. Furthermore, it can be observed that the maximum motion speed occurs at the throat, while speed decreases as the section area increases (also in the divergent side). This leads to the existence of a second equilibrium point (point $\mathcal{E}$ in Fig. 6), which is stable, located in the divergent section of the inlet at $A(\tilde{x}) = A_1$. Indeed, in the event of a disturbance at this second equilibrium point, the resulting speed tends to bring the shock wave back to that position, in contrast to what occurs at the first equilibrium point, located in the convergent part of the duct. It is assumed that the subsonic solution downstream is associated to a second throat with area A_t.

This result is consistent with the experiments conducted by Kantrowitz and Donaldson [12,15], and it provides a clear description of the start-up and hysteresis problems present in supersonic air inlets. In order to achieve a configuration with minimal losses, the normal shock wave should be positioned as close as possible to the throat. If, for a given geometry and inlet Mach number, the shock wave is detached and located in front of the inlet, the geometry must be modified in some way (such as using perforations or a variable geometry [25,26]) to increase the effective throat area, so that the curve corresponding to that Mach number lies above the KD limit. Under this condition, the shock wave will undergo autonomous start and settle at the stable equilibrium point in the divergent section, provided that there is a second throat downstream in critical conditions which controls the flow. Since the stagnation pressure losses in this configuration are significant,

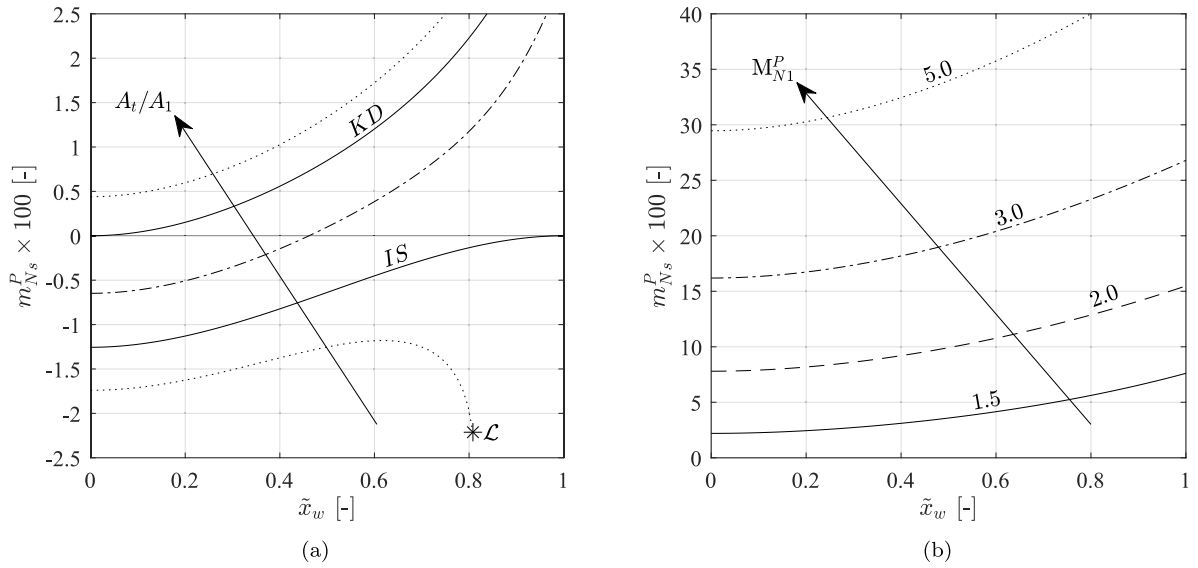

Fig. 5. Dimensionless motion speed of a normal shock wave, m^P_{Ns}, as a function of the dimensionless position of the shock wave, $\tilde{x}_w$, obtained for the sample inlet for: (a) an entrance Mach number $M^P_{N1} = 1.20$ and different values of the ratio between the throat area and the inlet area, A_t/A_1 (0.968, 0.971 (IS), 0.974, 0.978 (KD) and 0.980); and (b) a throat area ratio $A_t/A_1 = 0.95$ and different Mach numbers at the entrance. $\mathcal{L}$: limit where $A_w = A^{P*}$.

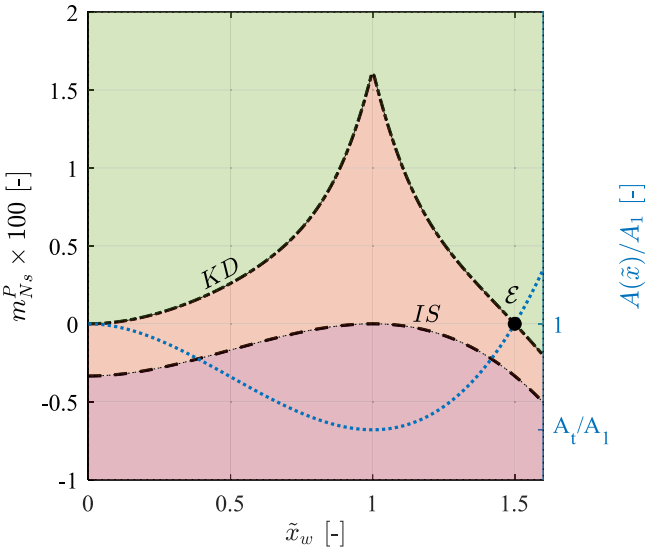

Fig. 6. Dimensionless motion speed of a normal shock wave, m^P_{Ns}, as a function of the dimensionless position of the shock wave, $\tilde{x}_w$, obtained for the inlet in Fig. 4 (blue) for an entrance Mach number $M^P_{N1} = 1.10$. IS limit and KD limit. Green: autonomous start region; orange: hysteresis; red: unstart. $\mathcal{E}$: stable equilibrium position. (For interpretation of the references to color in this figure legend, the reader is referred to the web version of this article.)

the second throat, which has critical conditions downstream, can be modified so that the stable equilibrium point moves closer to the throat. However, if the critical throat is closed below the IS limit, unstart occurs, and the shock wave will be expelled and once again be detached in front of the inlet.

4. Comparison with experimental results

The results from the experiments mentioned in Section 1.3 (see Table 1) are presented in the following paragraphs, and compared to those obtained using the DS^2M model developed in this paper. Five experimental works have been considered (see Table 1) corresponding to different configurations, Mach numbers, diagnostic means, and back-pressure generation devices. This election was not intentional, but was forced by the absence of more candidates. In order to make a meaningful comparison with the theoretical DS^2M model results, based on the stability change of the configuration, it is necessary to know the area of the critical throat at the onset of unstart, and also the Mach number of the flow feeding the normal shock wave in the supersonic region as it is expelled. Extracting these data from the information provided in the literature presents varying degrees of difficulty, making the analysis somewhat complex in some cases. Therefore, brief considerations are included in each case to describe the modelization required.

A first distinction between single-throat and double-throat ducts (see Sections 4.1 and 4.2) that makes the analysis significantly dissimilar is the associated variation in the configuration of the stability regions [35]. Furthermore, three-dimensional inlets (see Section 4.3) contribute to an increased complexity in the modelization. In addition, the effect of combustion is addressed in Section 4.4, providing further insight into the system behavior. Finally, buzz frequency can be explained considering the motion speed of shock waves, as shown in Section 4.5.

4.1. *Two-dimensional single-throat duct at* $M_\infty = 4.9$

Wagner et al. [34] analyzed the unstart dynamics in a two-dimensional inlet model tested in a supersonic wind tunnel (see Fig. 7), based on pressure measurements and Schlieren images. The tested inlet geometry consisted of a horizontal wall on the lower side and a wedge-shaped cowl. The entrance height was $H_0 = 35.1$ mm, followed by a 6° slope wedge. The duct featured a constant section (isolator) with $h = 25.4$ mm height until the exit, where a flap was placed. The flap consisted of a flat plate of thickness e, whose pivot axis was shifted a distance d from the end of the inlet and placed at an angle δ_f.

The effective cross-section area that allows the fluid to pass at the exit can be expressed as a function of the flap deflection angle as:

$$A_t(\delta_f) = \left(h - e\cos\delta_f - d\tan\delta_f\right)\cos\delta_f. \tag{21}$$

In these tests, the flap deflection was suddenly modified from a value of $\delta_f = 0°$ to the desired δ_f, observing whether the unstart took place or not. To analyze these experimental results, first it is necessary to calculate the flap deflection upon which the DS^2M model predicts negative shock wave motion speeds in the central region of the inlet

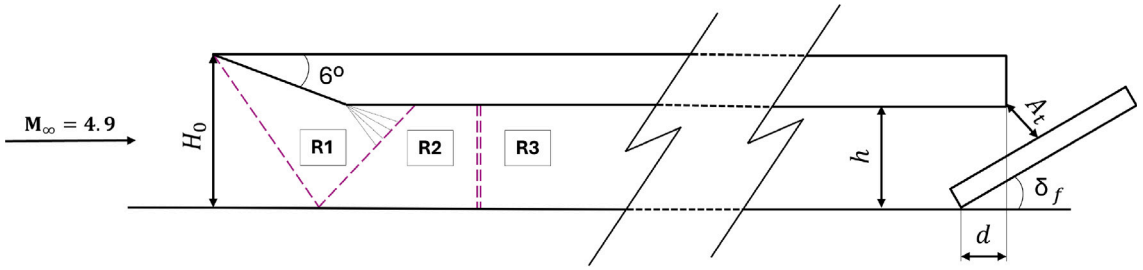

Fig. 7. Geometry and flow patterns for the inlet tested by Wagner et al. [34].

(associated with the unstart phenomenon) and compare it with the value at which unstart was observed during the tests.

A simplified flow pattern over the tested inlet is assumed, as shown in Fig. 7: two oblique shocks and a normal shock split the flow field into four regions. The first region, placed upstream of the first shock wave, corresponds to the undisturbed flow, where the Mach number is $M_\infty = 4.90$. Region $R1$, placed between the two oblique shocks, has a Mach number of $M_1 = 4.31$. In region $R2$, it is assumed that the flow is parallel to the walls, with a Mach number behind the second oblique shock wave of $M_2 = 3.83$. Finally, in region $R3$, downstream the normal shock wave, the Mach number will depend on downstream conditions, which, if the normal shock is static, is $M_3 \approx 0.42$. It is noteworthy that, according to Wagner et al. [33,34], the boundary layer thickness is considerable, so the previous calculations for the Mach numbers in the different regions are only approximations. Due to this uncertainty, another Mach number value, 20% lower, has also been considered in the DS^2M model to assess the influence of the Mach number on the theoretical results. This percentage has been chosen ensuring that, while it is not excessive, it is sufficiently large to account for uncertainties related to the boundary layer thickness effect. In fact, this value has been computed in such a way that with the adjusted Mach number value, the experimental results are expected to fall within the range predicted by the DS^2M model, as will be shown (see Fig. 8). Another contribution to the uncertainty is that the moving shock wave observed during the experiments was not a normal shock but a curved one (the normal Mach number is smaller).

The effect of the expansion fan generated in region $R1$ at the end of the wedge has been neglected, as the disturbances of the oblique shock waves observed in the Schlieren images (see Figure 4 of Wagner et al. [34]) are almost unnoticeable. This is due both to the typical isentropic nature of expansions in supersonic flow, which allows the stagnation properties to be preserved, and to the limited degree of expansion (given that $\delta = 6°$) which results in the Mach number remaining nearly unchanged.

Moreover, near the flap in the region close to the exit, the flow cannot be modeled as one-dimensional; thus, the effect of this region on the flow is modeled as an effective passage area, $A_t(\delta_f)$, which limits the flow rate that can pass through. Additionally, the potential unsteady effects of the rapid closure of the pass area when the flap is actuated are not considered, based on the authors' description that the closure speed of the flap does not affect the unstart.

Thus, for each value of flap deflection δ_f, the value of $A_t(\delta_f)$ can be obtained using Eq. (21), which in turn allows for calculating the ratio $A_t(\delta_f)/h = A_t/A_1$. Since during the tests the shock moved in a duct of constant section, the shock motion speed should also be a constant, and can be determined as a function of δ_f (see Fig. 8). The flap deflection δ_f for which unstart is predicted by the DS^2M model aligns reasonably well with that measured by Wagner et al. [34], $\delta_f = 28 \pm 3°$, mainly for $M_2 = 3.06$ (a 20% lower than the initially estimated value). The better fit for a lower Mach number could be attributed to the simplifications made along the modelization.

It must be considered that the effective throat area should be less than the geometric area due to the boundary layer effect, which would translate into larger effective flap angles (or smaller throat areas A_t), shifting the rectangle representing experimental results to the right in Fig. 8-(a) or to the left in 8-(b), bringing the experimental observations closer to the DS^2M model results.

In this same context, once the normal shock wave propagates upstream, the boundary layer may separate, resulting in a further reduction of the effective pass area, thus increasing the effective flap deflection. Therefore, the predicted upstream motion speed (in absolute value) of the normal shock wave increases until a steady state is reached, approaching the measured motion speed values between 19 and 37 m/s reported by Wagner et al. [34].

This idealization may seem too ambitious, as the real upstream moving shock in the duct is not a normal shock, but a curved one, as seen in the Schlieren images (see Figure 9 from Wagner et al. [34]), and also the thickness of the boundary layer at the inlet floor is noted to be substantial, according to these authors. In spite of these differences, theoretical and experimental results converge reasonably well, which can be justified by the results of the comparison of Tamaki et al. [46] (Section 5.1) between a pseudo-shock and an equivalent normal shock wave (where an effective normal shock wave at a reduced Mach number is considered).

4.2. *Two-dimensional double-throat duct at* $M_\infty = 4.0$

Rodi et al. [41] conducted a series of experimental tests to analyze the influence of back-pressure on the onset of unstart in the two-dimensional air inlet of a dual-mode ramjet/scramjet engine, obtaining speeds of 59.2 ± 3.7 m/s in the inlet duct (see Fig. 9). The inlet model tested is shown in Figures 1 and 2 of Rodi et al. [41], along with the pressure gauges (GX, $X = 1$ to 6) installed along the upper and lower walls of the inlet.

Among other results, Rodi et al. [41] recorded the time evolution of the pressure measured at each pressure gauge, and identified the pass of the shock wave. They estimated the average motion speed of the shock between two consecutive gauges, based on the time delay between the shock wave pass through successive gauges and the distance between them.

In this case, the difficulties of the analysis arise from determining both the critical area of the valve A_v at the onset of unstart, and the variation of the Mach number in the supersonic region that is swept by the normal shock as it is expelled. To establish these parameters, it is first necessary to identify the unstart process in this inlet, which requires developing a simplified model of both the geometry and the flow characteristics over the inlet, as shown in Fig. 9, where appropriate simplifications are proposed for a configuration with the normal shock located far downstream from the entrance section. The inlet geometry is modeled using a set of three consecutive ramps with increasing slopes (5°, 8°, and 12°, respectively), followed by a region of constant area (isolator). The cowl consists of a movable section of length L, followed by a horizontal wall. The movable part can rotate by an angle δ around its pivot axis. Additionally, there is a final mass flow control valve (flap) with area A_v.

The flow regions, bounded by the set of oblique shock waves considered, are also shown. The region upstream is unaffected by the

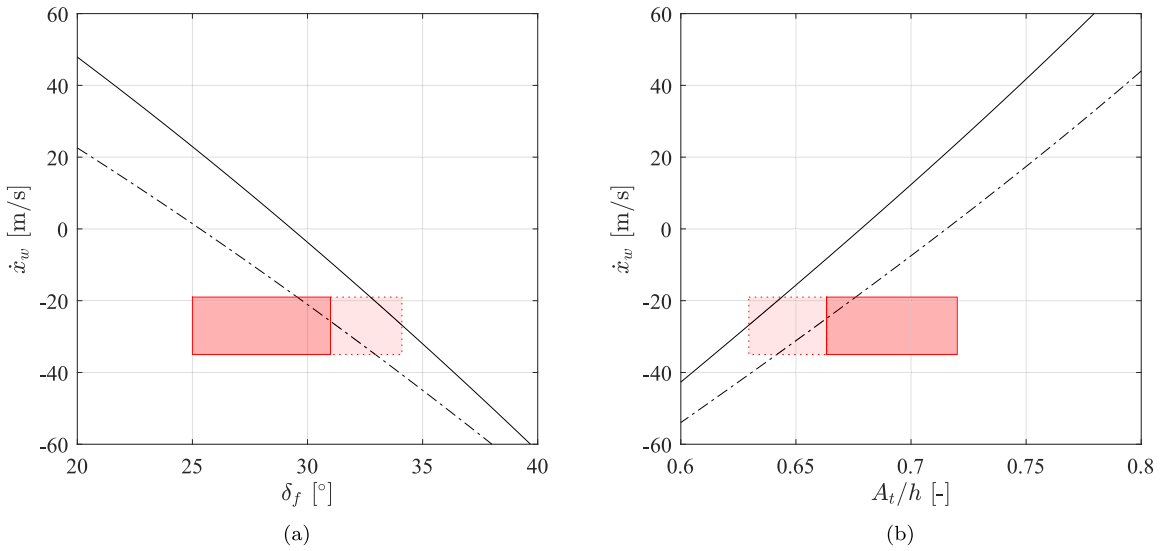

Fig. 8. Motion speed of a normal shock wave $\dot{x}_w$ (solid lines: $M_2 = 3.83$; dashed lines: $M_2 = 3.06$) in the constant section duct (isolator, see Fig. 7), as a function of the flap deflection angle δ_f (left); and as a function of A_t/h, the ratio of the effective passage area in the throat to the area of the constant section (right). Solid square: angle of unstart ($28 \pm 3°$) (horizontal side); and range of motion speeds measured experimentally (vertical side) from Wagner et al. [34]. Dotted red square: 10% increase in effective flap angle viscous effect trend (effective decrease in throat area).

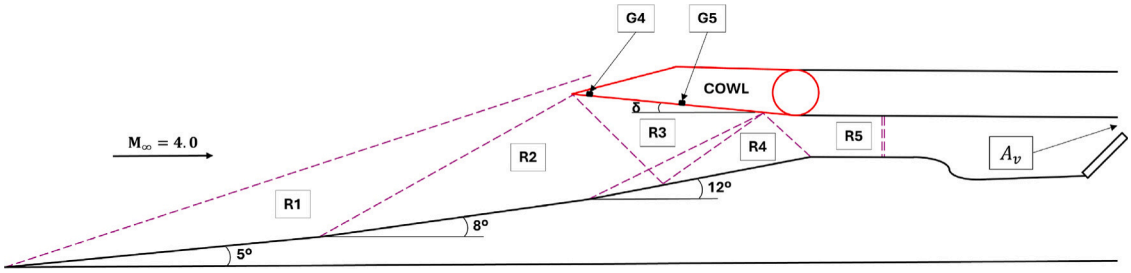

Fig. 9. Simplified geometry of Rodi et al. [41] supersonic inlet and flow patterns at the inlet.

Table 2
Mach numbers in the different regions of the flow (started flow). The Mach number in the region $R5$ is M_t, and behind the normal shock wave, it is $M_{t,d}$. A_t/A_v from Eq. (3), for $M_{t,d}$.

δ	Mach $R1$	Mach $R2$	Mach $R3$	Mach $R4$	Mach $R5$	$M_{t,d}$	A_t/A_v
6	3.64	3.45	2.63	1.84	1.41	0.736	1.071
0	3.64	3.45	2.98	2.39	1.91	0.594	1.196
−4	3.64	3.45	3.21	2.78	2.23	0.543	1.266
−6	3.64	3.45	3.33	2.99	2.40	0.523	1.298

presence of the inlet, with a freestream Mach number $M_\infty = 4.0$. Then, five regions ($R1$ to $R5$) appear due to the multiple reflections occurring outside and inside the inlet duct (background waves). It is assumed that downstream the last depicted region ($R5$) the flow is parallel to the walls, allowing only the possibility for a normal shock wave. Two additional regions emerge between regions $R2$ and $R4$, but their extent is considered negligible compared to the other regions. In this figure, the locations of the two pressure gauges ($G4$ and $G5$) can be found (see Figures 1 and 2 of Rodi et al. [41]). These two pressure gauges were used to estimate the shock wave motion speed (see experimental results in Fig. 10).

Using the relationships for oblique shock waves [20], the Mach number in each of these regions can be obtained. Specifically, assuming that a normal shock wave is located at the isolator throat (consistent with Figure 3 of Rodi et al. [41]), the results for regions $R1$ to $R5$ are presented in Table 2. This allows to estimate the critical area (valve area A_v) at the onset of unstart using $M_{t,d}$ and Eq. (3).

In brief, this problem (including the final valve) can be modeled as an open duct (see Fig. 11) with a set of oblique shock waves produced by the leading ramp (background waves [8]), followed by a closed duct with two throats (converging entrance-throat A_t-backward step-converging flap-final throat A_v). A wide range of flow patterns can arise during the system evolution, particularly due to the presence of the two throats [35]. This system exhibits a phenomenon of multi-stability associated with hysteresis during transitions between different flow patterns. In this case, assuming the second throat is always smaller than the first, $A_v < A_t$, there are only three possible flow patterns and a set of transitions (jumps) between them (see Fig. 11).

The flow pattern $P1$ occurs when the shut-off valve A_v has a sufficiently large area (though still smaller than A_t), resulting in supersonic flow throughout the duct without a normal shock wave (started flow). For a smaller valve area, pattern $P2$ appears, with the normal shock wave located in the diverging section of the inner duct. Finally, if the valve area is small enough, pattern $P3$ arises, with the normal shock wave located upstream of the inlet (the transition to $P3$ marks the onset of unstart).

Tao et al. [35] analyzed the possible appearance of hysteresis cycles associated with the transitions between these flow patterns.

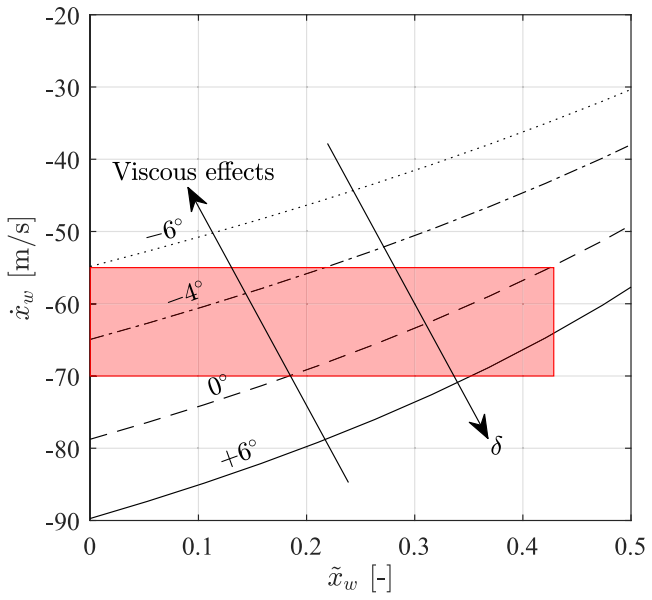

Fig. 10. Motion speed of a normal shock wave during unstart obtained from the proposed formulation. The valve area is critical for the outgoing Mach number of the normal shock wave located at the isolator throat. See Table 2. Red rectangle: experimental results from Rodi et al. [41].

These transitions are as follows. *Transition* 3 – 2: For a fixed Mach number and sufficiently small valve area, pattern $P3$ appears, with the normal shock wave detached upstream of the duct. As the valve area is gradually increased, the flow jumps to pattern $P2$, where the normal shock wave is ingested and located somewhere in the diverging section, with valve area A_v in critical conditions corresponding to the Mach number downstream of the background shocks. *Transition* 2 – 1: From this pattern, further increasing the valve area causes the normal shock to shift towards the exit along the diverging section, and when it reaches the maximum section, the normal shock becomes unstable, and it is swallowed by the valve A_v, and pattern $P1$ appears. *Transition* 2 – 3: Conversely, if starting from pattern $P2$ the valve area is reduced, the shock wave reaches throat A_t (with the valve area critical for the downstream Mach number $\mathrm{M}_{t,d}$), and the normal shock is expelled in the entrance converging section (as there it is unstable) and pattern $P3$ appears, with the shock wave detached upstream of the inlet. *Transition* 1 – 3: Finally, if the valve area is progressively reduced starting from pattern $P1$, unstart occurs as the valve becomes critical for the Mach number at the throat A_t, leading directly to pattern $P3$, without passing through pattern $P2$.

The question is, which transition (1 – 3 or 2 – 3) takes place in Rodi's experiments as the valve is closed? This is relevant for determining the critical throat area A_v that triggers unstart. To clarify this point, the shock wave position should be known in order to determine the Mach number of the flow downstream the shock. Fortunately, in Figure 3 (case 4) of Rodi et al. [41], the static pressure variation along the duct is presented, showing a shock wave near the throat in the configuration prior to unstart. Therefore, we assume that the nominal pattern in these experiments corresponds to the limit of pattern $P2$, with unstart occurring via transition 2 – 3. Since the shock wave is located at the throat A_t at the limit of pattern $P2$, we assume that the valve area required to generate this pattern is nearly equal (with a slight increment) to that which produces unstart, which is the critical area for the Mach number downstream the shock at the throat $\mathrm{M}_{t,d}$ (see Table 2 for different δ values). If the 1 – 3 transition had been chosen for the unstart, the critical area of the valve, A_v, corresponding to the Mach number in the region $R5$ should have been used, and the calculated values for the shock wave motion speed would have been significantly different.

The second step is to estimate the Mach number of the flow swept by the normal shock as it propagates upstream along its path through the duct as it is being expelled. To do this, a one-dimensional isentropic flow in a variable area duct is considered on the region between the lip edge and the throat, rather than considering the set of oblique shock waves that is replaced by the moving normal shock wave. The duct geometry is defined as follows. The inlet area, A_1, is measured from the leading edge of the inlet lip and along the local vertical. The throat area, A_t, is located in the constant section of region $R5$ (see Fig. 9). The valve area, A_v, represents the passage area at the end section of the inlet, corresponding to the non-obstructed area at the flap section depicted in Figure 1 of Rodi et al. [41].

The inlet area A_1 is a function of the deflection angle δ of the movable part of the cowl (considered positive when it increases the entrance area), that is:

$$\frac{A_1(\delta)}{A_t} = \frac{A_{1,\delta=0}}{A_t} + \frac{L_c}{A_t}\tan\delta, \tag{22}$$

where L_c is the length of the duct segment. Furthermore, in the duct segment that includes the movable cowl, the area law is given by:

$$\frac{A(\tilde{x};\delta)}{A_1} = 1 - \frac{A_t}{A_1(\delta)}\frac{L_c}{A_t}(\tan\theta + \tan\delta)\,\tilde{x}, \tag{23}$$

where $\tilde{x} = x/L$, with x being the longitudinal coordinate measured from the leading edge of the movable cowl of the inlet; and $\theta = 12°$ is the slope of the last ramp section of the inlet (see Fig. 9).

With the flow configuration shown in Fig. 9 and the Mach numbers obtained for region $R5$ in the cases of $\delta = 6°$, $\delta = 0°$, $\delta = -4°$, and $\delta = -6°$, the valve area can be determined for the normal shock to be placed at the throat A_t, as A_v should be critical conditions for $\mathrm{M}_{t,d}$. The results are presented in Table 2.

Since the data given by Rodi et al. [41] were acquired from gauges located at positions $G4$ and $G5$ (see Fig. 9), only the most upstream regions $R1$ and $R2$ (and the free stream) would remain unaffected during the pass of the normal shock through region $R3$. Therefore, to obtain the supersonic Mach number that the moving normal shock wave will face on its way upstream, an isentropic variation is considered, starting with a flow at a Mach number of 3.45 (the value in $R2$) in the inlet segment of a duct with the converging geometry described by Eq. (23). The DS^2M model results are shown in Fig. 10. The tendency accounted for viscous effects has also been included in that figure, presenting an improvement in the matching of the DS^2M model results compared with the experimental ones.

As Rodi et al. [41] do not clearly specify the speed of the shock as a function of the lip angle δ, it can only be confirmed that the ranges of measured speeds and theoretical results for the cowl angle range δ considered fit satisfactorily.

4.3. *Three-dimensional single-throat duct at* $\mathrm{M}_\infty = 5.3$

The experiment by Wieting et al. [40] was designed to study the structural loads that arise when unstart occurs. The geometry of the inlet consisted of a front part with wedge-shaped side walls, opened at the bottom side to facilitate shock wave ingestion and reduce spillage, and a closed downstream duct of constant cross-section, equipped with a pin whose insertion reduced the pass section and caused unstart. From an aerodynamic point of view, this inlet presents a significant complexity even during the started regime, as the leading oblique shock waves start from a leading edge that is not straight.

The shock motion speed data obtained by Wieting et al. [40] from two close pressure sensors is approximately 27 m/s in the rear zone, in front of the pin but within the closed duct, in the section of constant area (see Fig. 12). A schematic representation of the geometric characteristics is shown in Fig. 12 together with the simplified fluid configuration assumed for the numerical modeling.

The flow topology upstream of the normal shock wave is divided into three regions. First, there is the undisturbed flow upstream of

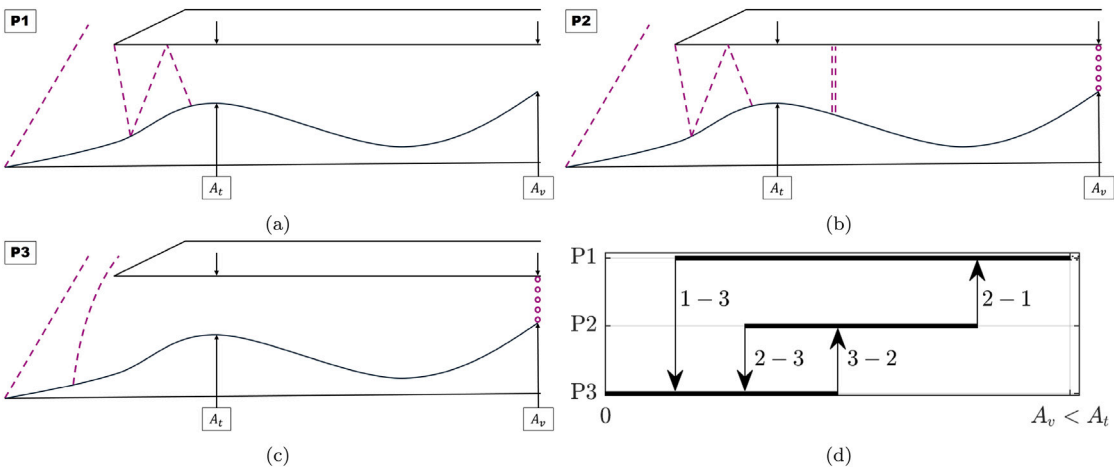

Fig. 11. Flow patterns $P1$ (a), $P2$ (b), and $P3$ (c), along with a diagram of the hysteresis process existing between the three flow patterns (d).

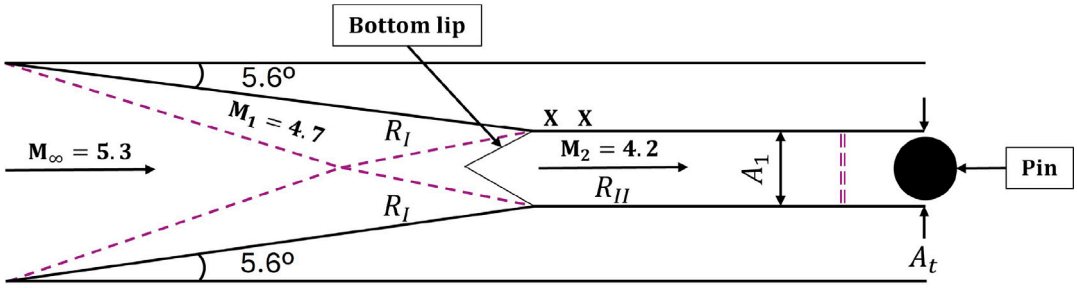

Fig. 12. Sketch of the geometric characteristics and simplified fluid configuration (plan view) of the inlet tested by Wieting et al. [40]. X: pressure sensors location.

the inlet, where the Mach number is $M_\infty = 5.3$. From the lip edges, two oblique shock waves develop, which limit two symmetric regions (denoted as R_I in Fig. 12) downstream, where the Mach number is $M_1 = 4.7$. Downstream, in the constant section area of the duct, region R_{II} appears, with the flow parallel to the walls and a Mach number of $M_2 = 4.2$. When the closing pin placed at the end of region R_{II} is inserted, leaving an effective pass area A_t, a shock wave (modeled as a normal one) is here generated. The shock moves upstream until it reaches the entrance section, facilitating spillage during unstart.

The determination of the effective pass area A_t is not straightforward. The difficulty arises from evaluating the data provided by the authors, as well as the potential relevance of viscous phenomena. Indeed, for unstart to occur at $M_2 = 4.2$, the theoretical critical area is given by $A^*/A_1 = 0.078$, which is far from the value $A^*/A_1 = 0.33$ reported by Wieting et al. [40], which would correspond to $M_2 = 2.64$ (a value that does not seem could be obtained with the shock wave system of Fig. 12). However, viscous effects may lead to an effective reduction in the throat area, bringing the experimental value of A^*/A_1 closer to the theoretical one.

Therefore, the analysis of the results from this experiment is limited to conducting a sensitivity study of the shock motion speed to parameters such as the throat-to-entry area ratio A_t/A_1 (varied in the range $0.2 - 0.6$), and the shock-to-entry area ratio A_w/A_1 (varied in the range $0.6 - 1.0$), comparing these results with those from Wieting et al. [40].

The motion speed of the normal shock wave, $\dot{x}_w$, is depicted in Fig. 13-(a) as a function of the ratio between the throat and entry areas, At/A_1, obtained using the present formulation for different values A_w/A_1. It also includes the speed of −27 m/s, associated with a point in the closed duct but near the bottom lip, measured by Wieting et al. [40]. According to the geometry, there may be some spillage behind the shock wave, resulting in a reduction of speed compared to that calculated for a closed duct. The Mach number at the inlet duct entrance, M^P_{N1}, as a function of the throat-to-entry area ratio, A_t/A_1, needed to achieve a shock motion speed of −27 m/s, for different values of the shock-to-entry area ratio, A_w/A_1, is shown in Fig. 13-(b).

According to results in Fig. 13, different scenarios can be considered. First, it seems that the curve corresponding to the normal shock wave passing through a section with an area $A_w/A_1 = 0.6$ (60% of the entry area) is the one that best fits the results of Wieting et al. [40]. However, it seems reasonable to think that the position where the speed of the normal shock wave is measured, located in the straight section, presents an effective area close to that of the entry, *i.e.*, $A_w/A_1 \approx 1$. If the value of the Mach number is the one calculated from the fluid configuration in Fig. 12 and the data provided by Wieting et al. [40] ($M^P_{N1} = 4.2$), then Fig. 13-(b) suggests that the effective throat area is between $A_t/A_1 = 0.55$ and $A_t/A_1 = 0.60$. However, if the throat area is the value provided by Wieting et al. [40], then the incident Mach number at the shock, M^P_{Nw}, is significantly greater than that estimated. Based on the drawings in Figure 3 of Wieting et al. [40], the first scenario (A_t/A_1 between 0.55 and 0.60) seems more reasonable than the second (significantly greater Mach number at the shock than estimated by Wieting et al. [40]). Therefore, it is quite likely that, during the pin insertion process, unstart began (for a value of A_t/A_1 between 0.55 and 0.60, greater than the final one) before the final position of the pin was reached (0.40 and 0.33, without and with viscous effects, respectively), and the shock motion speed was not affected by the subsequent reduction in throat area. Indeed, according to Wieting et al. [40], the pin insertion time was varied between 1.5 and 30 ms. Given the shock wave motion speed of 27 m/s reported by Wieting, the wave would travel a distance between 40 and 810 mm during the pin insertion period—equivalent to approximately 5.3 to 116.6 times the pin diameter, and between one-quarter and 4.5 times the total length of Wieting's model. Therefore, the shock wave is far enough from the pin insertion point from the onset of unstart conditions, such that any further insertion does not influence its motion speed.

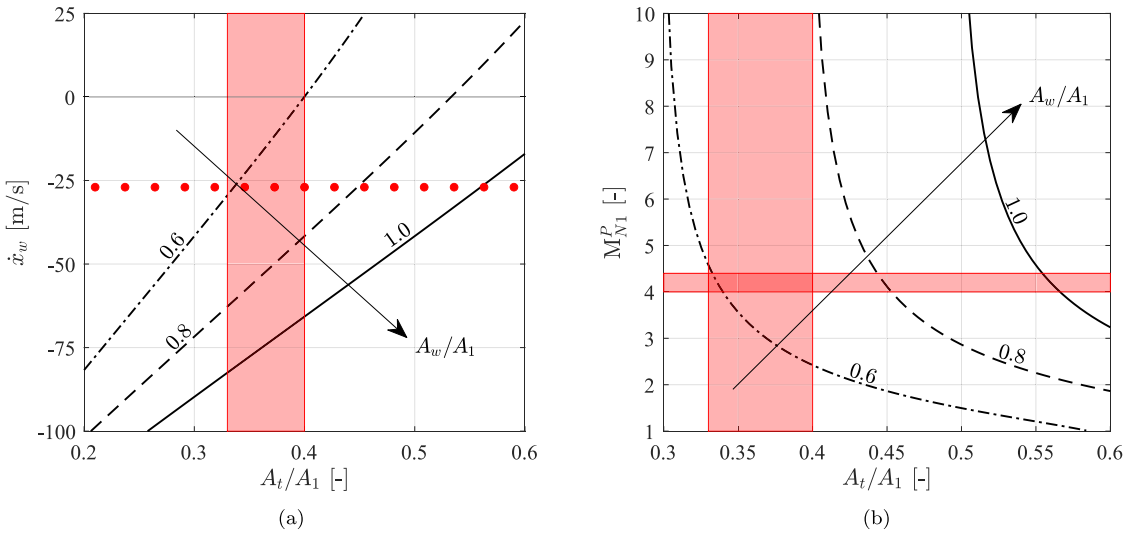

Fig. 13. (a) Motion speed of a normal shock wave, $\dot{x}_w$, as a function of the throat area-to-entry area ratio (At/A_1), obtained by the DS^2M model, for different values of the shock-to-entry area ratio, A_w/A_1; and (b) Mach number at the inlet, M^P_{N1}, as a function of the throat-to-entry area ratio (A_t/A_1), obtained by the DS^2M model, for a shock motion speed of $\dot{x}_w = -27$ m/s (Wieting et al. [40]), for different values of Aw/A_1. Circles: experimental data from Wieting et al. [40]. Shaded vertical regions: $A_t/A_1 = 0.40$ and 0.33 (without and with viscous effects, respectively, according to Wieting et al. [40]). Shaded horizontal region: $M^P_{N1} = 4.4$ and 4.0 (i.e., $M^P_{N1} = 4.2 \pm 5\%$).

4.4. Scramjet with combustion at $M_\infty = 5.5$

In the experiments of O'Byrne et al. [2] (see Figures 12 and 13 of O'Byrne et al. [2]), a scramjet at $M_\infty = 5.5$, there was no geometric closing valve, but rather the direct effect of increased back-pressure due to fuel ignition.

The reported speeds kept constant along the duct, and ranged between 75 and 150 m/s (for different values of the fuel–air ratio). Therefore, the order of magnitude of these speeds is compatible with the DS^2M model.

And, concerning the variation of shock speed along the duct, which has a constant section (see Figures 12 and 13 of O'Byrne et al. [2]), the shock speed remains constant, which is in agreement with the DS^2M model result that the shock speed depends on the duct area.

Potential variations in pressure in the subsonic region due to possible changes in combustion do not appear to have an influence either. A more detailed comparison would be possible if the relationship between the throat critical area and the fuel–air ratio were available.

4.5. Scramjet with buzz at $M_\infty = 4.9$

Another potential application of the DS^2M model is the analysis of the instability known as buzz. We will focus here on the experiments from Tan et al. [42,43]. They studied a hypersonic inlet at $M_\infty = 4.9$ as shown in Fig. 14, where the initial ramps have been omitted, and only the duct, composed of the isolator and combustor together with the control valve, has been included. The buzz results, providing the fundamental pressure oscillation frequencies for different cases, are given in Table 4 of Tan et al. [42] and Table 18 of Tan et al. [43]. In this last case, the throttling ratio is not directly given but should be interpolated from the initial and final time tags and initial and final throttling ratios data. In this way, the fundamental frequency of variation of the static pressure signal from some sensors can be related to A_v/A_1 from both papers [42,43].

Despite the complexity of the internal motion, due to the presence of the shock train, a simplification is made (modeling the shock train as an equivalent normal shock), subjected to a certain effective Mach number, M^P_{N1}. There are two sections of constant cross-section: the isolator (dimensions 100 mm × 10.5 mm) and the combustor (dimensions 90 mm × 16 mm). The motion speed of the normal shock observed by Tan et al. [42,43], can be deduced from the buzz frequency as $V_E = -2L_T f$, where L_T is the total length of the duct (isolator and combustor), and f is the buzz frequency. The mean speed can be calculated from the DS^2M model, V_M, through relation:

$$\frac{L_T}{V_M} = \frac{L_{iso}}{V_{iso}} + \frac{L_{comb}}{V_{comb}}, \tag{24}$$

where V_{iso} and L_{iso}, and V_{comb} and L_{comb} are the motion speeds of the shock wave and duct lengths in the isolator and combustor, respectively. To calculate both V_{iso} and V_{comb}, the reference section is considered to be the isolator, with area A_1, and an entrance Mach number in the range $1.6 < M^P_{N1} < 3.0$ (to account for uncertainties), which is obtained considering the incident Mach number, $M_\infty = 4.9$, and the effect of the subsequent inclined ramps ($M^P_{N1} \approx 2.3$). The area in the combustor is $A_{comb}/A_1 = 1.52$.

In the analysis performed, the time taken for the reconfiguration of shock waves in the forward ramp and the entrance of the inlet during spillage is neglected, as it is much shorter than the travel time of the shock within the duct. Tan et al. [42] observed that the travel times for shock swallowing and expelling were similar, so in the following, only the shock expelling speed is considered. The comparison of results (see Fig. 15) shows good consistency, and the results of the DS^2M model follow the trend of the experimental results when varying A_v/A_1. Therefore, it can be deduced that, for inlets presenting large length ducts, buzz frequencies are dominated by the mean speed of the shock traveling along the duct.

5. Conclusions

During the design phases of supersonic and hypersonic air inlets, it is of great interest to understand the potential occurrence of the unstart phenomenon, which is associated with a significant reduction in inlet performance. Additionally, it is important to identify the equilibrium positions of the normal shock wave located within the inlet duct, as well as to assess its stability. Furthermore, although theoretical models already exist, their considerable complexity justifies the development of an approximate theoretical model that enables rapid calculations.

Therefore, the interest of this paper is focused on the study of transient phenomena associated with the start and unstart of supersonic air inlets. To this end, the DS^2M model has been developed, which allows for approximate shock speed calculations, facilitating the search for equilibrium positions and the assessment of their stability, which is related to the duct geometry and incident Mach number. Furthermore,

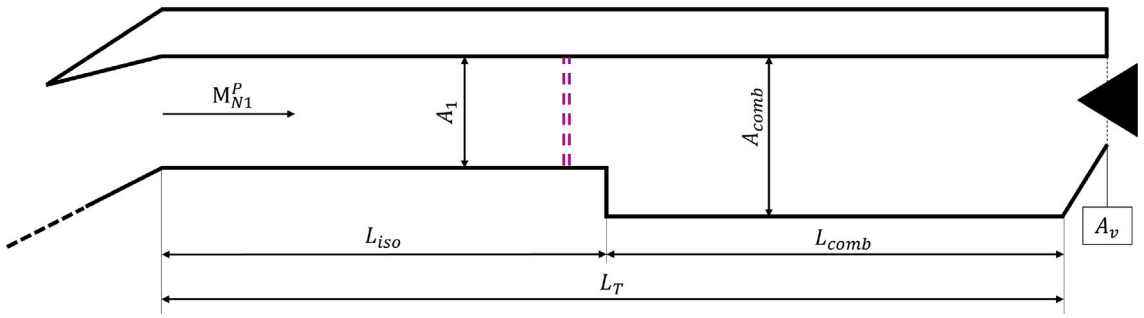

Fig. 14. Schematic representation of the geometric characteristics and flow of the inlet tested by Tan et al. [42,43].

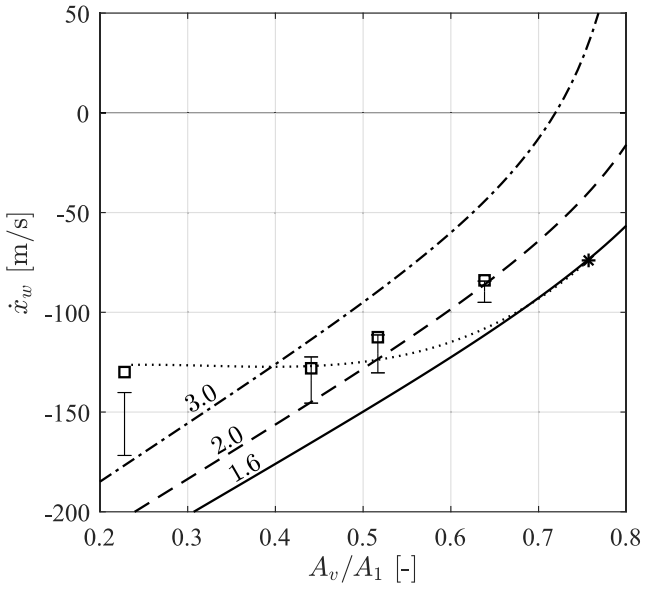

Fig. 15. Motion speed of a normal shock wave, $\dot{x}_w$, as a function of the ratio between the valve area and the inlet area (Av/A_1), obtained by the DS^2M model (V_M, Eq. (24)) for different Mach numbers, and obtained from the data (V_E) of Tan et al. [42] (symbols) and Tan et al. [43] (dotted line). Error bars: error range given by Tan et al. [42].

it has been shown that the DS^2M model can be applied to both supersonic and hypersonic inlets, provided the possibility of modeling the shock train by means of an equivalent normal shock wave.

The stability of the normal shock wave, when the configuration parameters exceed the Kantrowitz–Donaldson limit (the KD limit) or remain below the isentropic limit (the IS limit), and the instability (and hysteresis) in cases between these two limits, are well-known. However, one of the main contributions of this paper is to enter into details and provide results on the shock wave motion speed as a function of the main parameters involved (area ratio, Mach number, etc.).

The results obtained using the DS^2M model have been compared with experimental data reported by various authors—quantitatively when sufficient data were available. In such cases, the model demonstrated an acceptable level of agreement with experimental results. In other cases, where experimental data were limited or incomplete, the comparison was necessarily qualitative, with the objective of contributing to a better understanding of the underlying physical phenomena observed in the experiments.

The analysis has highlighted the critical importance of accurate experimental characterization to enable meaningful comparisons with theoretical predictions from the DS^2M model. Discrepancies in flow configurations and the presence of viscous effects—particularly boundary layer development and flow separation—have been shown to significantly influence the outcome of both experimental and theoretical analyses. Consequently, if the DS^2M model is to be employed for preliminary design purposes, these effects should be carefully characterized and accounted for, in order to ensure that the model's predictions reliably approximate real-world behavior.

The predictive capabilities of the DS^2M model are inherently constrained by the assumptions adopted in its formulation, as well as by the accuracy with which experimental conditions are represented. Nevertheless, the model has demonstrated strong qualitative and, when possible, quantitative agreement with experimental observations.

In the comparison with experimental results, the lack of comprehensive data in certain cases has required the introduction of assumptions and corrections—such as accounting for the influence of boundary layer thickness on the Mach number within the duct and on the effective throat area.

Furthermore, the presence of dual-throat configurations introduces an additional layer of complexity when attempting to determine the specific configuration responsible for triggering unstart. This issue arises particularly in scenarios where the effect of combustion in hypersonic inlets is considered, either through actual fuel burning or by increasing the back-pressure via a second throat.

The theoretical model developed in this work may also serve as a valuable tool for the design of experiments and for evaluating the diagnostic system requirements necessary to investigate hypersonic intake behavior.

CRediT authorship contribution statement

Carlos Carbajosa: Writing – review & editing, Writing – original draft, Validation, Software, Methodology, Investigation, Formal analysis, Data curation, Conceptualization. **Ángel Sanz-Andrés:** Writing – review & editing, Writing – original draft, Validation, Supervision, Project administration, Methodology, Investigation, Formal analysis, Conceptualization. **Alejandro Martínez-Cava:** Writing – review & editing, Supervision, Resources, Project administration, Funding acquisition, Conceptualization. **Mikel Ogueta-Gutiérrez:** Writing – review & editing, Writing – original draft, Supervision.

Declaration of Generative AI and AI-assisted technologies in the writing process

During the preparation of this work, the authors used ChatGPT in order to improve the translation and readability of the document. After using this tool, the authors reviewed and edited the content as needed and take full responsibility for the content of the published article.

Declaration of competing interest

The authors declare that they have no known competing financial interests or personal relationships that could have appeared to influence the work reported in this paper.

Acknowledgments

This work is part of the project TED2021-130541B-C21, funded by MCIN/AEI/10.13039/50110001103, the European Union "NextGenerationEU"/PRTR and project PID 2022-137630OB-C21 financed by MCIN/AEI/10.13039/501100011033/FEDER, UE. The work of Carlos Carbajosa has been supported by Programa Propio de I+D+i de la Universidad Politécnica de Madrid.

Appendix A. List of symbols

List of Symbols

Superscripts

^{B}	Subsonic branch.
^{P}	Supersonic branch.

Subscripts

$_0$	Initial time instant.
$_1$	Inlet entrance section.
$_\infty$	Upstream of the inlet, undisturbed flow.
$_d$	Downstream the shock wave, evaluated in the reference frame attached to the shock wave.
$_i$	Upstream the shock wave, evaluated in the reference frame attached to the shock wave.
$_N$	Magnitude referred to the reference frame attached to the inlet.
$_s$	Total or stagnation magnitude.
$_t$	Throat of the inlet.
$_v$	Valve (or second throat) of the inlet.
$_W$	Magnitude referred to the reference frame attached to the shock wave.
$_w$	Shock wave position.

Greek symbols

$\ddot{\chi}_w$	Dimensionless shock wave acceleration measured in the reference frame N.
δ	Deflection angle of the cowl moving part.
δ_f	Deflection angle of the rear moving part (or flap).
$\mathcal{E}$	Stable equilibrium point in the divergent section of the inlet.
η	Ratio between the area at a given section, A, and the area at the inlet entry section, A_1.
γ	Specific heat ratio of air.
$\mathcal{L}$	Limit of the parametric curves.
τ	Dimensionless time.
τ_c	Characteristic closure time.
θ	Slope of the last ramp section of the inlet.
ξ	Relative difference between inlet entry area and throat area, $1-\eta_t$.
$\mathcal{Z}$	Zero-speed curves.

Roman symbols

A	Area.
a	Speed of sound.
A^*	Critical area.
CR	Contraction ratio.
d	Flap pivot axis distance from the end of the inlet.
e	Flap thickness.
F	Prandtl's relationship associated function.
f	Buzz frequency.
GX	Pressure gauge number X.
H_0	Inlet entrance height.
h	Isolator height.
M	Mach number.
L	Longitudinal distance between the inlet entrance and the throat.
L_{char}	Characteristic length.
L_{comb}	Inlet combustor length.
L_c	Inlet duct segment length.
L_{iso}	Inlet isolator length.
L_T	Inlet duct total length (isolator and combustor).
m^P_{Ns}	Dimensionless shock wave motion speed with reference to the stagnation sound speed (reference frame N).
PX	Flow pattern number X.
R_g	Gas constant for air.
r_{Ts}	Ratio between T^P_{Ns} and T_{Ws}.
T	Temperature.
t_c	Characteristic closure time.
t_{ref}	Reference time.
t_r	Characteristic residence time.
V	Fluid speed.
V_{comb}	Combustor shock motion speed.
V_E	Experimental buzz equivalent speed.
V_{iso}	Isolator shock motion speed.
V_M	DS^2M model buzz mean speed.
x	Longitudinal coordinate measured from the inlet entrance.
$\ddot{x}_w$	Shock wave motion acceleration measured in axes fixed to the inlet.
$\dot{x}_w$	Shock wave motion speed (reference frame N).
$\tilde{x}$	Dimensionless longitudinal coordinate, x, scaled with L.

Appendix B. Conservation of enthalpy in fixed and moving reference frames

Once the complete problem has been solved (obtaining the shock motion speed), given an inlet geometry, an entrance Mach number, M^P_{N1}, and a specific position of the shock wave, $\tilde{x}_w$, the values of the remaining variables may be determined. In particular, the stagnation temperature downstream of the shock wave in reference frame N, T^B_{Ns}, can be obtained.

To achieve this, first, the Mach number at the supersonic side of the shock, M^P_{Nw}, can be obtained from:

$$\frac{A(\mathrm{M}^P_{Nw})}{A^*} = \frac{A_1}{A_1^*}\eta_w, \tag{B.1}$$

and at the subsonic side of the shock, M^B_{Nw}, from:

$$\frac{A(\mathrm{M}^B_{Nw})}{A^*} = \frac{\eta_w}{\eta_t}. \tag{B.2}$$

Furthermore, once the problem is solved and the dimensionless shock motion speed m^P_{Ns} is known, the ratio T^P_{Ns}/T^P_w can be obtained from (8). In addition, M^P_{Ww} can be obtained making use of Eq. (11), along with the previous results, which allows us to use Eq. (18) to find M^B_{Ww}. By employing Eq. (14), we obtain T_{Ws}/T^P_w, while the value of r_{Ts} can be determined using its definition given by Eq. (15), dividing T^P_{Ns}/T^P_w by T_{Ws}/T^P_w, both of which have been obtained previously. Through

$$\frac{T_{Ws}}{T^B_w} = 1 + \frac{\gamma-1}{2}\left(\mathrm{M}^B_{Nw} - \sqrt{r_{Ts}}\sqrt{\frac{T_{Ws}}{T^B_w}}m^P_{Ns}\right)^2, \tag{B.3}$$

the value of the ratio T_{Ws}/T^B_w can be derived, and by dividing T^P_{Ns}/T^P_w (Eq. (8)) by T_{Ws}/T^P_w (Eq. (14)) and multiplying the result by T_{Ws}/T^B_w (Eq. (B.3)), we obtain T^P_{Ns}/T^B_w. Finally, since the stagnation temperature at inlet reference frame downstream of the shock wave can be obtained from:

$$\frac{T^B_{Ns}}{T^B_w} = \frac{T^B_{Ns}}{T^P_{Ns}}\frac{T^P_{Ns}}{T^B_w} = 1 + \frac{\gamma-1}{2}\left(\mathrm{M}^B_{Nw}\right)^2, \tag{B.4}$$

the value of the ratio of stagnation temperatures upstream and downstream the shock wave at reference frame N, T^B_{Ns}/T^P_{Ns}, can be derived. To quantify this relationship of stagnation temperatures, the geometry shown in Fig. 4 is proposed, whose area law follows Eq. (20). Fig. B.16

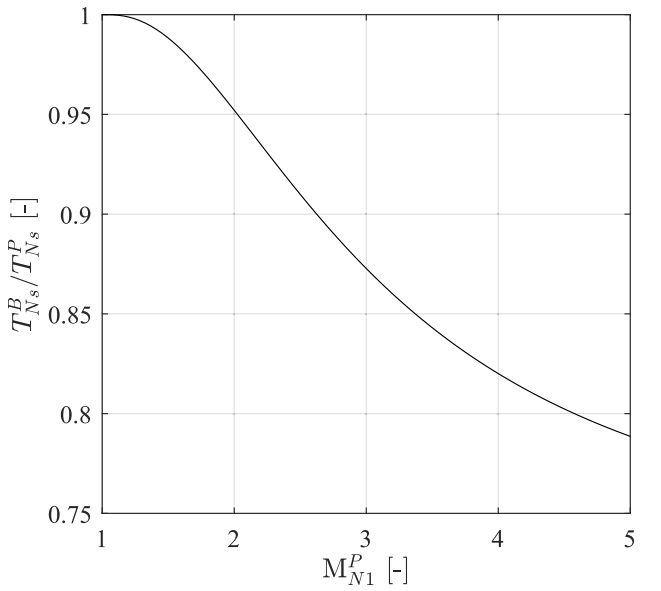

Fig. B.16. Variation of the ratio between the stagnation temperature downstream, $T^B_{N_s}$, and upstream, $T^P_{N_s}$, the shock wave at reference frame N as a function of the Mach number at the entrance, M^P_{N1}, for conditions corresponding to curve IS in the inlet of Fig. 4, when the shock wave is placed at the throat ($A_w = A_t$).

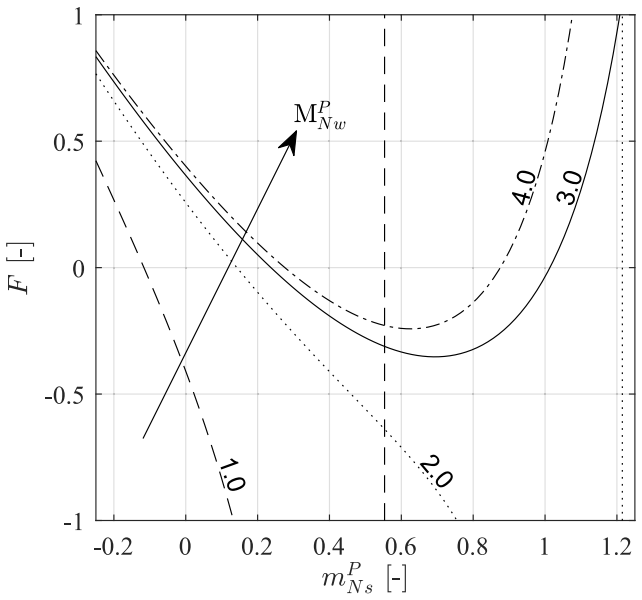

Fig. D.17. Prandtl's relation, F, as a function of the dimensionless shock motion speed, $m^P_{N_s}$, for several values of the Mach number at the supersonic side of the shock, M^P_{Nw}.

illustrates the evolution of the stagnation temperature ratio, T^B_{Ns}/T^P_{Ns}, as a function of the Mach number at the inlet, M^P_{N1}, for a configuration $A_t/A_1(M^P_{N1})$ corresponding to curve IS in the inlet of Fig. 4 when the shock is located at the throat. It can be observed that the stagnation temperature is approximately conserved, although this statement becomes less accurate as the Mach number increases.

Appendix C. Determination of the acceleration and position of the normal shock wave

Once the motion speed of the shock wave has been obtained, the dimensionless acceleration can be derived as follows:

$$\ddot{\chi}_w = \frac{\mathrm{d}m^P_{Ns}}{\mathrm{d}\tau} = \frac{\mathrm{d}\tilde{x}_w}{\mathrm{d}\tau}\frac{\mathrm{d}m^P_{Ns}}{\mathrm{d}\tilde{x}_w} = m^P_{Ns}\frac{\mathrm{d}m^P_{Ns}}{\mathrm{d}\tilde{x}_w}, \tag{C.1}$$

where the dimensionless time $\tau = t/t_{ref}$ has been used, and $t_{ref} = L/\sqrt{\gamma R_g T^P_{Ns}}$ is the reference time. Considering that $m^P_{Ns} = m^P_{Ns}(\eta_w; M^P_{N1}, \eta_t)$, Eq. (C.1) provides the following functional relationship:

$$\ddot{\chi}_w = \ddot{\chi}_w(\tilde{x}_w; M^P_{N1}). \tag{C.2}$$

The acceleration in dimensional form is given by:

$$\ddot{x}_w(\tilde{x}_w; M^P_{N1}, T^P_{Ns}, L) = \frac{\gamma R_g T^P_{Ns}}{L}\ddot{\chi}_w(\tilde{x}_w; M^P_{N1}). \tag{C.3}$$

The position of the shock wave is given by:

$$\tau(\tilde{x}_w; M^P_{N1}, \tilde{x}_{w,0}) = \int_{\tilde{x}_{w,0}}^{\tilde{x}_w} \frac{\mathrm{d}\tilde{x}_w}{m^P_{Ns}(\tilde{x}_w; M^P_{N1})}. \tag{C.4}$$

which can be solved once both the shock wave motion speed and the initial position $\tilde{x}_{w,0}$ are known.

Appendix D. Caveats on the solution of the Prandtl's relation

To obtain the motion speed of the shock wave relative to the stagnation sound speed at the reference frame N, $m^P_{N_s}$, the zeros of the problem defined by Eqs. (11), (12) and (18) should be determined. Specifically, it is necessary to find the value of $m^P_{N_s}$ that cancels the function F, defined as:

$$F\left(m^P_{N_s}; \eta_w, M^P_{N1}, \eta_t\right) = \left(M^B_{Ww}\right)^2 - \frac{1 + \frac{\gamma-1}{2}\left(M^P_{Ww}\right)^2}{\gamma\left(M^P_{Ww}\right)^2 - \frac{\gamma-1}{2}}. \tag{D.1}$$

Note that the zeros of Eq. (D.1) coincide with those of Eq. (18). From the previous expression, it can be deduced that if $M^P_{Ww} \geq 1$, then $(\gamma-1)/(2\gamma) \leq \left(M^B_{Ww}\right)^2 \leq 1$, and considering that the flow direction is from the entrance to the throat, it follows that $\sqrt{(\gamma-1)/(2\gamma)} \leq M^B_{Ww} \leq 1$. By differentiating Eq. (D.1) with respect to $m^P_{N_s}$, we obtain:

$$\frac{\partial F}{\partial m^P_{Ns}} = \frac{\left(\gamma^2+1\right)M^P_{Ww}}{\left[\gamma\left(M^P_{Ww}\right)^2 - \frac{\gamma-1}{2}\right]^2}\frac{\partial M^P_{Ww}}{\partial m^P_{Ns}} + 2M^B_{Ww}\frac{\partial M^B_{Ww}}{\partial m^P_{Ns}}. \tag{D.2}$$

From the previous expression, the derivatives of the incident and outgoing Mach numbers of the shock can be obtained from Eq. (11) and Eq. (12), respectively, yielding:

$$\frac{\partial M^P_{Ww}}{\partial m^P_{Ns}} = -\sqrt{\frac{T^P_{Ns}}{T^P_w}} < 0, \tag{D.3}$$

and

$$\frac{\partial M^B_{Ww}}{\partial m^P_{Ns}} \approx -\sqrt{r_{T_s}\frac{T_{Ws}}{T^B_w}} < 0. \tag{D.4}$$

In the last expression, second-order effects derived from the dependence of the temperature ratios on $m^P_{N_s}$ have been neglected. Since all temperatures are always positive, and the air flows from the entrance to the throat (there is no reverse flow), the Mach numbers will be positive, and thus the slope of the function F, given by Eq. (D.2), should be negative:

$$\frac{\partial F}{\partial m^P_{Ns}} < 0. \tag{D.5}$$

The evolution of F as a function of the dimensionless shock motion speed, m^P_{Ns}, is shown in Fig. D.17 for various values of the Mach number at the supersonic side of the shock at reference frame N, M^P_{Nw}. Two solutions of $F = 0$ for each Mach number appear, although only the one with negative slope is valid (see Eq. (D.5)).

References

[1] E.T. Curran, W.H. Heiser, D.T. Pratt, Fluid phenomena in scramjet combustion systems, Annu. Rm. Fluid. Mech. 28 (1996) 18, http://dx.doi.org/10.1146/annurev.fl.28.010196.001543.

[2] S. O'byrne, M. Doolan, S.R. Olsen, A.F.P. Houwing, Analysis of transient thermal choking processes in a model scramjet engine, J. Propuls. Power 16 (5) (2000) 808–814, http://dx.doi.org/10.2514/2.5645.

[3] N. Mushtaq, P. Gaetani, Understanding and modeling unstarting phenomena in a supersonic inlet cascade, Phys. Fluids 35 (2023) http://dx.doi.org/10.1063/5.0160706.

[4] D.M. Van Wie, Scramjet inlets, in: Scramjet Propulsion, American Institute of Aeronautics and Astronautics, 2001, pp. 447–511, http://dx.doi.org/10.2514/5.9781600866609.0447.0511.

[5] J. Chang, N. Li, K. Xu, W. Bao, D. Yu, Recent research progress on unstart mechanism, detection and control of hypersonic inlet, Prog. Aerosp. Sci. 89 (2017) 1–22, http://dx.doi.org/10.1016/j.paerosci.2016.12.001.

[6] V.I. Zvegintsev, Gas-dynamic problems in off-design operation of supersonic inlets (review), Thermophys. Aeromechanics 24 (2017) 807–834, http://dx.doi.org/10.1134/S0869864317060014.

[7] S. kyun Im, H. Do, Unstart phenomena induced by flow choking in scramjet inlet-isolators, Prog. Aerosp. Sci. 97 (2018) 1–21, http://dx.doi.org/10.1016/j.paerosci.2017.12.001.

[8] H. xia Huang, H. jun Tan, F. bo Li, X. bin Tang, Y. Qin, L.B. Xie, Y.Y. Xu, C. min Li, S. min Gao, Y. Zhang, S. Sun, D. Zhao, A review of the shock-dominated flow in a hypersonic inlet/isolator, Prog. Aerosp. Sci. 143 (2023) http://dx.doi.org/10.1016/j.paerosci.2023.100952.

[9] J. Chang, Y. Fan, W. Bao, D. Yu, Y. Shen, Unstart margin control of hypersonic inlets, Acta Astronaut. 66 (1) (2010) 78–87, http://dx.doi.org/10.1016/j.actaastro.2009.05.021.

[10] J. Chang, R. Zheng, L. Wang, W. Bao, D. Yu, Backpressure unstart detection for a scramjet inlet based on information fusion, Acta Astronaut. 95 (2014) 1–14, http://dx.doi.org/10.1016/j.actaastro.2013.10.010.

[11] X. Jiao, J. Chang, Z. Wang, D. Yu, Hysteresis phenomenon of hypersonic inlet at high Mach number, Acta Astronaut. 128 (2016) 657–668, http://dx.doi.org/10.1016/j.actaastro.2016.08.025.

[12] A. Kantrowitz, C. duP. Donaldson, Preliminary Investigation of Supersonic Diffusers, Tech. Rep. Adv. confid. report L5D20, NACA, 1945.

[13] C. Tao, Z. Lv, D. Yu, Multistability and complex routes of supersonic inlet start/unstart, J. Propuls. Power 27 (2011) 1204–1211, http://dx.doi.org/10.2514/1.B34235.

[14] J. Zhang, L. Lin, G. Luan, W. Bao, Experimental research on the stability margin of a variable geometry scramjet combustor in wide flight conditions, Acta Astronaut. 202 (2023) 151–156, http://dx.doi.org/10.1016/j.actaastro.2022.10.008.

[15] A. Kantrowitz, The Formation and Stability of Normal Shock Waves in Channel Flows, Tech. Rep. Tech. Note 1225, NACA, 1947.

[16] G.B. Whitham, Linear and Nonlinear Waves, Wiley-Interscience, 1973, p. 636.

[17] W. Chester, The propagation of shock waves in a channel of non-uniform width, Quart. J. Mech. Appl. Math. 6 (4) (1953) http://dx.doi.org/10.1093/qjmam/6.4.440.

[18] R.F. Chisnell, The motion of a shock wave in a channel, with applications to cylindrical and spherical shock waves, J. Fluid Mech. 2 (3) (1957) 286–298, http://dx.doi.org/10.1017/S0022112057000130.

[19] G.B. Whitham, On the propagation of shock waves through regions of non-uniform area or flow, J. Fluid Mech. 4 (1958) 337–360, http://dx.doi.org/10.1017/S0022112058000495.

[20] Z. Han, X. Yin, Shock dynamics, Vol. 11, Springer Netherlands, Dordrecht, 1993, http://dx.doi.org/10.1007/978-94-017-2995-6, Ch. 6.

[21] W. Chester, The propagation of shock waves along ducts of varying cross section, Adv. Appl. Mech. 6 (1960) 119–152, http://dx.doi.org/10.1016/S0065-2156(08)70111-X.

[22] R. Tahir, Analysis of Shock Dynamics in Supersonic Intakes (Ph.D. thesis), McGill, Montréal, Québec, Canada, 2008.

[23] JHU-APL, Handbook of Supersonic Aerodynamics, Section 17: Ducts, Nozzles and Diffusers, Tech. rep., NAVWEPS report 1488, Vol. 6, 1964.

[24] J. Seddon, E. Goldsmith, Intake Aerodynamics, in: AIAA Education Series, American Institute of Aeronautics and Astronautics, 1985.

[25] J.C. Evvard, J.W. Blakey, The Use of Perforated Inlets for Efficient Supersonic Diffusion, Tech. Rep. Research Memo. E7C26, NACA, 1947.

[26] A. Najafiyazdi, R. Tahir, E.V. Timofeev, S. Mölder, Analytical and numerical study of flow starting in supersonic inlets by mass spillage, in: 43rd AIAA/ASME/SAE/ASEE Joint Propulsion Conference & Exhibit, AIAA, 2007, http://dx.doi.org/10.2514/6.2007-5072.

[27] J. Kang, F. Song, Y. Wu, D. Zhang, J. Zhou, X. Sun, Experimental study on the suppression of inlet blockage in rotating detonation combustor by porous-wall, Acta Astronaut. 225 (2024) 477–488, http://dx.doi.org/10.1016/j.actaastro.2024.09.030.

[28] W.-Y. Su, Y. Chen, F.-R. Zhang, P.-P. Tang, Control of pseudo-shock oscillation in scramjet inlet-isolator using periodical excitation, Acta Astronaut. 143 (2018) 147–154, http://dx.doi.org/10.1016/j.actaastro.2017.10.040.

[29] Y. Jin, Y. Zhang, X. Li, H. Tan, S. Sun, Suppression of flow response hysteresis in the throttling/unthrottling process for supersonic inlet, Acta Astronaut. 202 (2023) 34–47, http://dx.doi.org/10.1016/j.actaastro.2022.09.052.

[30] A. Pathak, P. Khare, V. Kulkarni, Impact of energy deposition as active flow control on scramjet inlet performance using Immersed Boundary Method, Acta Astronaut. 224 (2024) 291–308, http://dx.doi.org/10.1016/j.actaastro.2024.08.023.

[31] F. Wang, P. Fan, J. Zhang, Y. Fan, J. Yan, Preventing inlet unstart in air-breathing hypersonic vehicles using adaptive backstepping control with state constraints, Acta Astronaut. 211 (2023) 498–509, http://dx.doi.org/10.1016/j.actaastro.2023.06.043.

[32] D.M. Van Wie, F.T. Kwok, R.F. Walsh, Starting characteristics of supersonic inlets, Am. Inst. Aeronaut. Astronaut. Inc. (1996) http://dx.doi.org/10.2514/6.1996-2914.

[33] J.L. Wagner, A. Valdivia, K.B. Yuceil, N.T. Clemens, D.S. Dolling, An experimental investigation of supersonic inlet unstart, in: 37th AIAA Fluid Dynamics Conference and Exhibit, AIAA, 2007, http://dx.doi.org/10.2514/6.2007-4352.

[34] J.L. Wagner, K.B. Yuceil, A. Valdivia, N.T. Clemens, D.S. Dolling, Experimental investigation of unstart in an inlet/isolator model in Mach 5 flow, in: AIAA Journal, Vol. 47, 2009, pp. 1528–1542, http://dx.doi.org/10.2514/1.40966.

[35] C. Tao, Y. Daren, C. Juntao, B. Wen, Catastrophe model for supersonic inlet start/unstart, J. Aircr. 46 (2009) 1160–1166, http://dx.doi.org/10.2514/1.38926.

[36] R. Throckmorton, J.A. Schetz, L.S. Jacobsen, Experimental and computational investigation of a dynamic starting method for supersonic/hypersonic inlets, in: 48th AIAA Aerospace Sciences Meeting Including the New Horizons Forum and Aerospace Exposition, AIAA, 2010, http://dx.doi.org/10.2514/6.2010-589.

[37] B. Sun, K.Y. Zhang, Empirical equation for self-starting limit of supersonic inlets, J. Propuls. Power 26 (2010) 874–875, http://dx.doi.org/10.2514/1.46798.

[38] W.Z. Xie, W. Yang, Y. Jin, S. Yang, C. Zeng, S. Guo, Prediction of self-starting limit of two-dimensional supersonic inlets considering viscous effects, Aerosp. Sci. Technol. 106 (2020) http://dx.doi.org/10.1016/j.ast.2020.106229.

[39] Y. Jin, S. Sun, H. Tan, Y. Zhang, H. Huang, Flow response hysteresis of throat regulation process of a two-dimensional mixed-compression supersonic inlet, Chin. J. Aeronaut. 35 (2022) 112–127, http://dx.doi.org/10.1016/j.cja.2021.06.013.

[40] A.R. Wieting, Exploratory Study of Transient Unstart Phenomena in a Three-Dimensional Fixed-Geometry Scramjet Engine, Tech. Rep. TN D-8156, NASA, 1976.

[41] P.E. Rodi, S. Emami, C.A. Trexler, Unsteady pressure behavior in a ramjet/scramjet inlet, J. Propuls. Power 12 (1996) 486–493, http://dx.doi.org/10.2514/3.24061.

[42] H.-J. Tan, S. Sun, Z.-L. Yin, Oscillatory flows of rectangular hypersonic inlet unstart caused by downstream mass-flow choking, J. Propuls. Power 25 (1) (2009) 138–147, http://dx.doi.org/10.2514/1.37914.

[43] H.-j. Tan, L.-g. Li, Y.-f. Wen, Q.-f. Zhang, Experimental investigation of the unstart process of a generic hypersonic inlet, AIAA J. 49 (2) (2011) 279–288, http://dx.doi.org/10.2514/1.J050200.

[44] J. Lee, S.H. Kang, Numerical study on the start and unstart phenomena in a scramjet inlet-isolator model, PLoS ONE 14 (2019) http://dx.doi.org/10.1371/journal.pone.0224994.

[45] K. Matsuo, Y. Miyazato, H.D. Kim, Shock train and pseudo-shock phenomena in internal gas flows, Prog. Aerosp. Sci. 35 (1999) 33–100, http://dx.doi.org/10.1016/S0376-0421(98)00011-6.

[46] T. Tamaki, Y. Tomita, R. Yamane, A study of pseudo-shock, Bull. JSME 13 (55) (1970) 51–58, http://dx.doi.org/10.1299/jsme1958.13.51.

[47] M. Sajben, J.F. Donovan, M.J. Morris, Experimental investigation of terminal shock sensors for mixed-compression inlets, J. Propuls. Power 8 (1992) 168–174, http://dx.doi.org/10.2514/3.23457.

[48] M.R. Soltani, A. Daliri, J.S. Younsi, Effects of shock wave/boundary-layer interaction on performance and stability of a mixed-compression inlet, Sci. Iran. B 23 (4) (2016) 1811–1825, http://dx.doi.org/10.24200/sci.2016.3928.

[49] D.G. MacMartin, Dynamics and control of shock motion in a near-isentropic inlet, J. Aircr. 41 (2004) 846–853, http://dx.doi.org/10.2514/1.416.

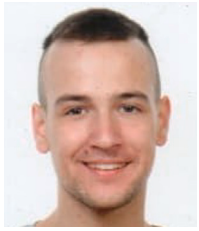

Carlos Carbajosa Ph.D. student in Aerospace Engineering, specializing in flight dynamics, aerodynamics, fluid dynamics, and computational fluid mechanics. Holds a Bachelor's and Master's degree in Aerospace Engineering from the Universidad Politécnica de Madrid (UPM). As a member of the research group at the Instituto Universitario de Microgravedad "Ignacio Da Riva" (IDR/UPM), have contributed to various projects in computational fluid mechanics and aerodynamics, including wind tunnel testing. Additionally, have imparted lectures on aerodynamic subjects at the Escuela Técnica Superior de Ingeniería Aeronáutica y del Espacio (ETSIAE), UPM.

Ángel Sanz-Andrés Full professor at Universidad Politécnica de Madrid (UPM), teaching Aerodynamics and Spacecraft Technology. Director of the Instituto Universitario "Ignacio Da Riva" (IDR/UPM) from 2016–2024. Research in Space technology: technical director of the small satellite program of UPM, and contributions to thermal and structural design of several instruments for scientific space missions. Concerning applied aerodynamics theoretical and experimental contributions in industrial applications. Published the results obtained in more than 105 international papers, 17 national publications, 69 proceedings, 22 books or book chapters, 2 patents and 70 technical reports, and have been the advisor of 22 Ph.D. Dissertations related to the above research fields.

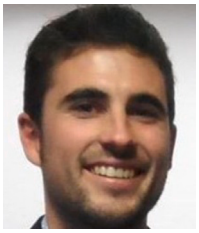

Alejandro Martínez-Cava From a combined experimental and numerical approaches, has a strong expertise in aerodynamics, CFD, flow control and hydrodynamic stability holding a Ph.D. in Aerospace Engineering at UPM (Madrid). As a member of NuMath and IDR/UPM research groups, he conducts both research and industry collaboration activities, getting involved in a wide range of applications. Besides his teaching activities in aerodynamics (for undergrad and master courses), his research joins numerical analyses and wind tunnel testing on the analysis of low and high speed flows.

Mikel Ogueta-Gutiérrez Mikel Ogueta is a researcher at the Instituto Universitario de Microgravedad "Ignacio da Riva", and a Lecturer in Aerodynamics at Universidad Politécnica de Madrid. Ph.D. with honors in Aeronautical Engineering. His research is mainly focused on wind tunnel testing and wind engineering. He has participated in more than 100 projects of wind tunnel testing of structures such as bridges, roofs, solar trackers, high-rise and low-rise buildings and such.